LIMNOLOGY
and
OCEANOGRAPHY: METHODS

Limnol. Oceanogr.: Methods 2022

doi: 10.1002/lom3.10501

Comparison of spectrophotometric and electrochemical pH measurements for calculating freshwater pCO_2

Fischer L. Young, Qipei Shangguan, Cory M. Beatty, Makenzy D. Gilsdorf, Michael D. DeGrandpre*
Department of Chemistry and Biochemistry, University of Montana, Missoula, Montana

Abstract

Inland waters have an important role in the global carbon cycle, contributing significantly to terrestrial carbon fluxes through downstream export and exchange of CO_2 with the atmosphere. However, large uncertainties in freshwater inorganic carbon fluxes remain. One contributing factor is uncertainty in carbonate system calculations for estimating the partial pressure of CO_2 (pCO_2) from pH and alkalinity in freshwater systems. The uncertainty stems largely from inaccurate pH values caused by glass pH electrode measurements in low ionic strength systems. This study compares indicator-based spectrophotometric and electrochemical pH measurements and their application for calculating freshwater pCO_2. Our study found that, compared to a pCO_2 reference method, pH electrode-based estimates of pCO_2 were overestimated by 230 ± 200 μatm ($n = 54$) where indicator-based spectrophotometric pH estimates of pCO_2 were 58 ± 33 μatm ($n = 34$) over the range of 100–1600 μatm. Furthermore, we found that when ionic strength was assumed to be zero, calculated pCO_2 error was $\sim 20\%$ of the reference pCO_2. A 19-d field study using autonomous spectrophotometric pH and pCO_2 sensors found an average error in calculated pCO_2 of -70 ± 57 μatm ($n = 1685$). Although, our focus is on riverine CO_2, these findings and subsequent conclusions apply to all freshwater systems. Spectrophotometric pH measurements will improve future freshwater pCO_2 calculations and better quantify inland waters' role in the global carbon budget.

Inland waters process and transport substantial amounts of terrestrially derived carbon (Hotchkiss et al. 2015). Most streams and rivers are sources of carbon dioxide (CO_2) to the atmosphere (Raymond et al. 2000; Wang and Cai 2004; Chen et al. 2012), where they represent a substantial component in the global carbon cycle (Cole et al. 2007; Raymond et al. 2013; Hotchkiss et al. 2015). A common way of evaluating the magnitude of these CO_2 sources is by calculating the CO_2 exchange over a given area of freshwater (i.e., flux). Current challenges in quantifying air–water CO_2 fluxes include obtaining accurate gas transfer velocities and accurately quantifying dissolved CO_2, usually reported as the partial pressure of CO_2 (pCO_2) (Raymond et al. 2012; Duvert et al. 2018; Rocher-Ros et al. 2019; Ulseth et al. 2019). Recent studies have outlined techniques to increase the accuracy of gas transfer velocities (Appling et al. 2018a,b; Rocher-Ros et al. 2021); however, debates continue about the best practices for obtaining accurate freshwater pCO_2 (Hunt et al. 2011; Abril et al. 2014; Liu et al. 2020).

Currently, freshwater pCO_2 is either measured directly or calculated. Researchers measure pCO_2 directly using in situ sensors (Parker et al. 2007; Lynch et al. 2010; Rocher-Ros et al. 2020) or headspace equilibrium techniques coupled to nondispersive infrared (NDIR) analysis or gas chromatography (Cole and Caraco 2001; Johnson et al. 2009; Åberg and Wallin 2014; Abril et al. 2015; Rocher-Ros et al. 2019; Aho et al. 2021). However, most freshwater studies rely on analysis of collected samples. The pCO_2 is then calculated from any two quantifiable inorganic carbon parameters, that is, total alkalinity (A_T), pH, or dissolved inorganic carbon (DIC). The two measured parameters are input into an equilibrium model that uses proton (i.e., A_T) and mass (i.e., DIC) balances and the thermodynamic equilibria for carbonic acid (H_2CO_3) (e.g., CO2SYS or PHREEQC) (Choi et al. 1998; Lewis and Wallace 1998; Butman and Raymond 2011; Parkhurst and Appelo 2013; Abril et al. 2014, 2015).

Both A_T and pH are commonly monitored by government and research agencies around the world (Raymond et al. 2013;

*Correspondence: michael.degrandpre@umontana.edu

Additional Supporting Information may be found in the online version of this article.

Stets et al. 2017; Wen et al. 2017; Coles et al. 2019; Liu et al. 2020) and these long-term datasets have been used to calculate pCO_2 and estimate global CO_2 emissions (Cole et al. 2007; Aufdenkampe et al. 2011). Studies have shown, however, that using A_T and electrochemical pH can result in overestimation of calculated pCO_2 leading to inflated estimates of global freshwater CO_2 emissions (Herczeg and Hesslein 1984; Hunt et al. 2011; Abril et al. 2015; Liu et al. 2020). Freshwater pCO_2 can be overestimated by 10% to > 100% when calculated from pH and A_T (Hunt et al. 2011; Abril et al. 2015; Liu et al. 2020). These erroneously high pCO_2 values are thought to be caused by systematically low electrode pH and the presence of non-carbonate species (e.g., organic acid anions) that can contribute to higher A_T values. This "excess A_T" overestimates pCO_2 because carbonate equilibrium models assume that freshwater A_T is all carbonate alkalinity. Other chemical species, like phosphate, could also contribute to A_T but are typically at negligible concentrations in freshwater compared to carbonate concentrations. Findings from Liu et al. (2020) revealed that organic acids can be a significant portion of A_T when A_T is less than $\sim 1000\ \mu$mol L^{-1} with errors in calculated pCO_2 of > 40%. This error is significantly reduced (< 8%), however, at higher A_T (e.g., > 2000 μmol L^{-1}; Liu et al. 2020). In addition, Liu et al. (2020) suggested empirical relationships based on ionic strength (μ) and dissolved organic carbon (DOC) to correct past electrochemical pH and A_T measurements, respectively. Even with the pH measurement correction, pCO_2 error was only reduced by $\sim$ 40% (Liu et al. 2020), so there remains a need for more accurate pH measurements and more rigorous thermodynamic calculations of pCO_2.

The inaccuracy of pH electrodes in freshwater is primarily due to changes in the liquid junction potential (Illingworth 1981; Herczeg and Hesslein 1984; Davison and Woof 1985; Stauffer 1990; Raymond et al. 1997). Calibration of an electrode in standard buffer solutions (i.e., National Institute of Standards and Technology [NIST]) that have higher μ than freshwater (i.e., μ > 0.01 M) commonly leads to systematically low pH in low μ conditions (Herczeg and Hesslein 1984; Byrne et al. 1988; French et al. 2002; Liu et al. 2020). Spectrophotometric pH, which uses a colorimetric indicator to determine pH, has demonstrated improved accuracy compared with glass electrodes (Byrne et al. 1988; Yao and Byrne 2001; French et al. 2002; Yuan and DeGrandpre 2008; DeGrandpre et al. 2014; Lai et al. 2016; Minor et al. 2019). The accuracy has been reported to be < 0.008 pH units for freshwater applications (Yuan and DeGrandpre 2008; Lai et al. 2016). Although spectrophotometric pH is commonly used for calculation of pCO_2 in seawater where its utility has been extensively characterized (Byrne et al. 1988; Zhang and Byrne 1996; Lueker et al. 2000; Byrne et al. 2010; DeGrandpre et al. 2014; Bockmon and Dickson 2015; Takeshita et al. 2020), it has not been significantly used for calculation of freshwater pCO_2 or for that matter, calculation of other freshwater equilibria (e.g., solubility). Freshwater measurements of spectrophotometric pH pose unique challenges, however, because of the uncertainty of μ effects and the potential perturbation of pH of poorly buffered freshwater by addition of indicator (Yuan and DeGrandpre 2008). Therefore, it is important to evaluate the utility of spectrophotometric pH measurements more thoroughly for freshwater applications, especially for its use in calculating pCO_2.

The recent availability of purified meta-cresol purple (*p*mCP) and characterization of its equilibrium constant at low μ has made this evaluation more opportune (Lai et al. 2016) where pH accuracy might vary due to different mCP impurities in commercial products (Liu et al. 2011). Over a decade ago, marine chemists discovered that dye impurities degrade the accuracy of seawater pH measurements and demonstrated improved accuracy by purifying the indicator (Yao et al. 2007; Liu et al. 2011). The effects of dye impurities on freshwater measurements have never been determined and so the uncertainty created by this problem has likely compromised the appeal of indicator-based pH measurements for freshwater. In addition, μ is integral to this assessment because it can alter the inorganic carbon equilibria, that is, the apparent dissociation constants increase with increasing μ (Stumm and Morgan 2008). The effect of μ on freshwater CO_2 calculations has not been rigorously evaluated, however. In addition, μ encompasses a range from $\sim$ 0.1 mM to > 10 mM in freshwater systems (Cormier et al. 2013), a range that significantly changes the apparent Henry's Law constant (K'_H), apparent dissociation constants (K'_1, K'_2, and K'_W) and, as a result, calculated pCO_2. Therefore, rigorously accounting for freshwater μ could improve carbonate equilibrium models and, accordingly, calculated pCO_2 values.

To evaluate the freshwater applicability of spectrophotometric pH measurements, a laboratory study was conducted to compare spectrophotometric and electrochemical pH measurements for calculating freshwater pCO_2 over a wide range of conditions (i.e., μ, A_T, and temperature). The experiments used a test tank where the pCO_2 could be monitored while samples were simultaneously obtained for pH and A_T. Furthermore, high-frequency in situ spectrophotometric pH measurements were made in a local river to evaluate the accuracy of calculating pCO_2 through a real-world application.

Materials and procedures

Laboratory tank study

Overview

A 130-L, temperature-controlled, well-mixed tank of a mixture of tap water and deionized (DI) water was sampled with pCO_2 ranging from $\sim$ 100 to 1600 μatm. The pCO_2 levels were varied by (1) introducing air that was passed through a column of soda lime (Fisher Scientific, CAS # 8006-28-8) to drive the pCO_2 below atmospheric levels ($\sim$ 100–400 μatm) or (2) introducing small volumes of high CO_2 into the test tank headspace to increase the pCO_2. A range of A_T from ~ 1800 to 3200 μmol L^{-1} and μ from ~ 5 to 9 mmol L^{-1} were created by dilution of tap water (undiluted tap water A_T = ~ 3200 μmol L^{-1}) in the tank with DI water. The tank temperature was set to 10°C, 15°C, or 20°C. Most data were collected at 15°C with a limited number of measurements made at 10°C and 20°C to determine performance over a broader temperature range. These conditions are like those found in a nearby river, the Clark Fork River (CFR), where we have worked extensively (Parker et al. 2007; Lynch et al. 2010; Shangguan et al. 2021), and other temperate and tropical freshwater rivers (Abril et al. 2015).

The tank pCO_2 was quantified using a membrane equilibrator (Membrana, Liqui-Cel SP Series) attached to a pump and a CO_2/H_2O infrared gas analyzer (LI-COR, LI-840A). The gas analyzer was zeroed with CO_2-free air and then calibrated with two CO_2 standards (359 and 1774 ppm) (Dickson et al. 2007). Sample collection began at the lowest pCO_2 concentration in the test tank (~ 100 μatm) and continued sequentially in ~ 150–200 μatm steps until ~ 1600 μatm. The pCO_2 was recorded on a 1-min interval and the measured mole fraction of CO_2 was converted to pCO_2 following Dickson et al. (2007). The overall tank pCO_2 accuracy is estimated to be ~ ± 5 μatm.

Samples for analysis of A_T and pH were collected to coincide with the equilibrator-infrared measurements. Triplicate samples were dispensed via a pump from the closed test tank to maintain pCO_2 levels. Samples were collected in borosilicate glass bottles secured with greased hollow glass stoppers. The samples were kept on ice for ~ 5–15 min until spectrophotometric pH and A_T analysis. For the pH electrode measurements, two additional samples (one for each pH electrode measurement) were collected immediately after the previously mentioned triplicate samples and analyzed within 1–2 min of sample collection.

Spectrophotometric pH

Spectrophotometric pH measurements were made using a double beam spectrophotometer (Agilent, Cary 300) with 10 cm borosilicate glass cuvettes and temperature regulated cuvette holders (Lai et al. 2016). Each bottle was analyzed only once to prevent an increase in headspace that could allow gas exchange and alter the pH and pCO_2. Triplicate spectrophotometric pH measurements were averaged for further analysis.

For freshwater pH analysis, *p*mCP was used because the negative logarithm of its acid dissociation constant (pK_a) is equal to 8.6607 at 25°C at infinite dilution (μ = 0 mM) (Lai et al. 2016) and overlaps with the pH range observed in the CFR (e.g., 7.9–9.1) (Parker et al. 2007) and many other alkaline freshwater systems (Peter et al. 2014). The pK_a for purified phenol red has also been quantified at low μ and would be suitable for a lower pH range (pK_a = 8.0625 at 25°C at infinite dilution) (Lai et al. 2016). Automated diagnostic checks were performed monthly on the spectrophotometer that included validation of wavelength accuracy, wavelength reproducibility, photometric noise, and baseline flatness, some of which have been shown to affect spectrophotometric pH measurement accuracy (DeGrandpre et al. 2014).

Spectrophotometric pH measurements were calculated on the free hydrogen ion scale ($pH_{free} = -\log[H^+]$, where $[H^+]$ is the hydrogen ion concentration) using the following equation (Yao and Byrne 2001; Lai et al. 2016):

$$pH_{free} = pK_a + \log\left(\frac{R - e_1}{e_2 - Re_3}\right) - 4A\left(\frac{\sqrt{\mu}}{1 + \sqrt{\mu}} - 0.3\mu\right) \quad (1)$$

where pK_a is the temperature-dependent negative logarithm of the 2nd dissociation constant of *p*mCP at infinite dilution. The indicator (I) *p*mCP exists in two forms in natural waters, the protonated (acid) form, HI^-, and the deprotonated (base) form, I^{2-}. Thus, R is the ratio of indicator absorbances (A_{578}/A_{434}) at the absorbance maxima of I^{2-} (578 nm) and HI^- (434 nm), e_1, e_2, and e_3 refer to the molar absorption coefficient ratios corresponding to HI^- and I^{2-} at 434 and 578 nm, and

$$A = 0.5092 + (T - 298.15) \times 8.5 \times 10^{-4} \quad (2)$$

where T is the temperature in Kelvin. Due to minor changes in pH of the sample caused by the addition of indicator (Seidel et al. 2008; Yuan and DeGrandpre 2008; Li et al. 2020), pH was calculated using a linear regression of the pH values recorded with addition of three 80 μL indicator aliquots. The magnitude of this perturbation correction was −0.005 ± 0.004 pH units (n = 84), similar to previously reported perturbation corrections (Yuan and DeGrandpre 2008). This procedure gave absorbances within a range of 0.0930–1.4740. Example pH values with relevant parameters (i.e., molar absorptivity, absorbance, temperature, and pK_a) are summarized in Supporting Information Table S1. All sample measurements were temperature corrected to the tank water temperature using the equilibrium model CO2SYS (Lewis and Wallace 1998) at infinite dilution (Millero 1979). This program uses an input (measurement) and output (tank) temperature, alkalinity, and input pH. Temperature corrections averaged −0.005 ± 0.004 pH units. The resulting temperature corrected pH was used for subsequent pCO_2 calculations and pH comparisons (see below). In addition, pH values from the spectrophotometer were compared bimonthly to an NIST traceable phosphate buffer (pH 8.00 ± 0.02 at 25.1 ± 0.3°C, μ = ~ 0.2 M) (Micro Essential Laboratory, Inc., Hydrion). The spectrophotometric pH measurements were converted to the National Bureau of Standards (NBS) scale (pH_{NBS}) (*see* below), and temperature corrected to 25.0°C. Measurements showed good agreement with the pH buffer (average error of −0.006 ± 0.02 pH units, n = 12, at 25.1 ± 0.3°C).

All spectrophotometric pH_{free} measurements were converted to pH_{NBS} using Eq. 3 (Stumm and Morgan 2008) to make them directly comparable with the electrochemical pH_{NBS} data. Note that in Eq. 3, z is equal to 1 (i.e., charge of the hydrogen ion).

$$pH_{NBS} = pH_{free} + Az^2\left(\frac{\sqrt{\mu}}{1+\sqrt{\mu}} - 0.3\mu\right) \tag{3}$$

Equation 3 indicates that pH_{free} and pH_{NBS} are related by the Davies term (i.e., $Az^2\left(\frac{\sqrt{\mu}}{1+\sqrt{\mu}} - 0.3\mu\right)$). At zero ionic strength both pH values are equal; however, as ionic strength increases, the Davies term also increases, and consequently, pH_{NBS} becomes greater than pH_{free}.

Tap water ionic strength was determined assuming the reported average ion concentrations from the Missoula aquifer (AWQR 2020; Supporting Information Table S2) and using the following equation (Stumm and Morgan 2008):

$$\mu = \frac{1}{2}\sum\left(c_i z_i^2\right) \tag{4}$$

where c_i and z_i are the concentration and charge of an ionic species, respectively. To determine the diluted tap water μ, we used a dilution factor derived from the undiluted and diluted specific conductivity and μ. Conductivity was measured using an in situ conductivity data logger (HOBO, Onset U24 Freshwater). The conductivity logger was calibrated with a 1000 μS cm^{-1} conductivity standard (Bicca, Catalog # 2237). Discrete measurements of conductivity were also taken for quality control using a handheld water quality meter (YSI Inc., Pro1030), hereafter referred to as the YSI that was calibrated in the same way as the in situ conductivity sensor. The undiluted and diluted calculated μ were used for all pH (Eqs. 1 and 3) and pCO_2 calculations as described below.

Electrochemical pH

Glass pH electrode measurements were made with two different electrodes: (1) an electrode commonly used for pH measurements in the field (YSI Inc., Pro1030) and (2) a laboratory grade pH electrode (Metrohm AG, Ecotrode Plus), hereafter referred to as Metrohm. Both electrodes were calibrated with 4.00, 7.00, and 10.00 NIST traceable pH buffers (Micro Essential Laboratory, Inc., Hydrion) to align with literature methods (Hunt et al. 2011; Abril et al. 2014) and the U.S. Geological Survey (USGS) recommended method for calibration (Barnes 1964). All water samples and calibration buffers were stirred and both pH electrode measurements were made immediately upon collection after a 1-min stabilization period. Sample temperature was measured at the same time as pH measurements to a precision of $\pm$ 0.1°C. To test their accuracy and precision after calibration, results of replicate ($n = 10$) buffer pH (8.00 $\pm$ 0.02 at 25°C) measurements were 7.99 $\pm$ 0.02 and 8.012 $\pm$ 0.009, for the YSI and Metrohm pH electrodes, respectively. During the study, the YSI and Metrohm pH electrodes had average response slopes of 98.1 %$\pm$ 0.1% (n = 6) and 100.1% $\pm$ 0.7% (n = 18), respectively, of the theoretical response.

Electrochemical pH measurements were temperature corrected to the in situ tank temperature using the same approach as outlined above for spectrophotometric pH. YSI pH measurements were only evaluated at ~ 15°C in the test tank because it was not available when tank measurements were being done at 10°C and 20°C.

Total alkalinity

Unfiltered samples were analyzed for A_T using an open cell titration system consisting of a syringe pump (Kloehn Co LTD), pH electrode (Metrohm AG, Ecotrode Plus), and pH meter (Fisher Scientific, AR 25). The electrode was conditioned for low ionic strength solutions by immersion in tap water for 1 h prior to use. Titration data were processed using the non-modified Gran Plot titration method (Gran 1952) from pH 3.5 to 3.1. The HCl acid titrant ranged from 0.0997 to 0.1002 N (Fisher Scientific) and the factory certified value was used in the analysis. A_T was analyzed on the bottle samples after spectrophotometric pH to minimize pH error from CO_2 exchange.

The automated titration system was tested monthly prior to sample analysis using an in-house alkalinity standard made from dried sodium carbonate (Na_2CO_3). The average difference between the standard and measured values was -1.0 ± 4.3 μmol L^{-1} (n = 13) (Supporting Information Fig. S1). Consequently, very good "calibration-free" accuracy was achieved, and no offsets were added to the standard A_T values.

DOC was measured on tank samples to assess whether non-carbonate alkalinity (i.e., organic acid anions) could be significant. DOC was analyzed with an Aurora 1030W Total Organic Carbon Analyzer (Xylem Inc., OI Analytical) that uses heated persulfate wet chemical oxidation coupled with an NDIR detector (U.S. EPA 2005).

Carbonate system equilibrium programs

Two commonly used equilibrium programs (CO2SYS and PHREEQC) (Lewis and Wallace 1998; Parkhurst and Appelo 2013) and an in-house MATLAB script (Supporting Information Appendix A) (hereafter referred to as CalcCO2_frompH) were used to assess the influence of μ on freshwater pCO_2 calculations. CO2SYS's freshwater option sets $\mu = 0$ (infinite dilution) (Lewis and Wallace 1998) while PHREEQC (Parkhurst and Appelo 2013) and CalcCO2_frompH can incorporate μ values. Carbonic acid thermodynamic equilibrium constants (K_1 and K_2) from Millero (1979) and Henry's law constant (K_H) from Weiss (1974) are used in CO2SYS and CalcCO2_frompH. CalcCO2_frompH accounts for changes in dissociation constants due to μ using the Davies equation (right side of Eq. 3) (i.e., apparent dissociation constants K'_1, K'_2, and K'_H; Supporting Information Appendix A). PHREEQC (version 3.4.0, database used: wateq4f; Ball and Nordstrom 1991), on the other hand, uses equilibrium constants from Plummer and

Busenberg (1982). Over a temperature range of 0–30°C, average percent differences between Millero (1979) and Plummer and Busenberg (1982) equilibrium constants (K_1 and K_2) were $0.15\% \pm 0.08\%$ and $0.25\% \pm 0.09\%$, respectively. Furthermore, the average percent difference between Weiss (1974) and Plummer and Busenberg (1982) Henry's law constant over the same temperature range was $0.18\% \pm 0.12\%$. These differences have a negligible effect on calculated pCO_2 so the pCO_2 from each equilibrium program can be directly compared. Input parameters for CO2SYS include in situ temperature, A_T, and in situ pH_{NBS}. PHREEQC uses the same input parameters as CO2SYS with the addition of μ that it estimates from A_T. To minimize the charge balance equation within PHREEQC, a counterion (sodium, Na^+, in this case) is used. Lastly, CalcCO2_frompH uses temperature, A_T, in situ pH_{free}, and the estimated μ explained above. pH_{free} is used instead of pH_{NBS} in CalcCO2_frompH to be consistent with the program's apparent dissociation constants.

Field application

Overview

In situ spectrophotometric pH measurements were made in the CFR to evaluate the accuracy of calculating pCO_2 through a real-world application. Submersible Autonomous Moored Instruments (DeGrandpre et al. 1995; Martz et al. 2003; Lynch et al. 2010) were deployed to measure spectrophotometric pH (SAMI-pH) and pCO_2 (SAMI-CO_2) directly in the CFR. A conductivity sensor for estimating μ was also deployed as described below. A conductivity-derived A_T was calculated from a linear relationship between specific conductivity and A_T obtained from data collected from 2017 to 2020 (discussed below). The calculated A_T was used with in situ pH_{free}, temperature, and μ to calculate pCO_2 using the CalcCO2_frompH program. This pCO_2 was then compared to the in situ pCO_2 measurements. A similar strategy is commonly used to compute seawater pCO_2, that is, A_T is derived from a linear relationship with salinity and used with pH measurements to compute pCO_2 (Gray et al. 2012; DeGrandpre et al. 2019). In situ temperature was measured directly from the SAMI-CO_2 and SAMI-pH. Temperature between the two sensors showed good agreement (-0.5 ± 0.4°C), so in situ temperature from the SAMI-pH was used for all sensor-related equilibrium calculations. Discrete bottle samples for A_T and spectrophotometric pH_{free} along with specific conductivity, pH_{NBS}, and temperature (YSI) were also collected four times during the deployment. This study took place from August 21, 2019 to September 9, 2019 during base flow river conditions on the CFR at Gold Creek (GC) (46°35′24″N, 112°55′42″W).

Autonomous in situ pH and pCO_2 *instruments*

The in situ pH system is based upon spectrophotometric pH measurements of sample and colorimetric indicator (e.g., purified meta-cresol purple), where a pump and valve draw in samples and mix with indicator (Seidel et al. 2008). The weak-acid indicator can perturb the sample pH and so the SAMI-pH employs an automated indicator pH perturbation correction (Seidel et al. 2008; Yuan and DeGrandpre 2008) like what was described above for discrete spectrophotometric pH measurements (Li et al. 2020). The in situ pCO_2 sensor also uses a colorimetric pH indicator (bromothymol blue) for spectrophotometric detection and operates by equilibration of ambient freshwater (or seawater) pCO_2 with the indicator contained in a gas-permeable membrane (DeGrandpre et al. 1995). Prior to the field deployment, both the pH and pCO_2 instruments were validated or calibrated in house, respectively. An NIST traceable pH 8.00 ± 0.02 at 25.0 ± 0.1°C ($\mu = \sim 0.2$ M) phosphate buffer was used to check the SAMI-pH accuracy. The SAMI-pH values were converted to pH_{NBS} (Eq. 3) and showed good agreement with the phosphate buffer (average error of -0.007 ± 0.001 pH units, $n = 12$, at 25.05 ± 0.05°C). The CO_2 sensor was calibrated over a range of 100–2000 μatm at 20.0 ± 0.1°C for 10 d in the same test tank described above, using the LI-COR for pCO_2 validation (DeGrandpre et al. 1995). The SAMI-CO_2 has a response time of ~ 5 min and an estimated uncertainty of $\sim 10 \pm 1$ μatm based on the standard deviation of residuals from the calibration fit ($n = 956$).

Conductivity and conductivity-derived alkalinity

The conductivity sensor (HOBO, Onset U24 Freshwater) was calibrated before deployment and assessed for sensor drift after deployment using the same method described above for the laboratory tests. Discrete measurements of conductivity were also taken using the YSI calibrated the same way as the in situ conductivity sensor. No sensor drift was evident but the entire in situ time series was corrected with a constant offset of -12.9 μS cm^{-1} based on the average difference between the in situ and discrete conductivity measurements.

The linear relationship using data collected from 2017 to 2020 at the deployment site ($n = 33$) between conductivity and A_T is shown in Fig. 1. A_T correlates with conductivity because it is primarily bicarbonate (HCO_3^-) at this location and is relatively conservative with a single source (i.e., groundwater) that is also diluted or concentrated proportionally from precipitation and evaporation, respectively. The residual error from this relationship ranged from -303 to $262\,\mu$mol L^{-1} with a standard deviation of $\pm 130\,\mu$mol L^{-1} ($\sim$5% uncertainty relative to the mean A_T). The contribution of A_T uncertainty to the calculated pCO_2 used for the field application is assessed below.

Estimating riverine μ

In situ μ was estimated using a relationship between A_T and μ at Bearmouth on the CFR from Nagorski (2001):

$$\mu = \left(2.63 \times 10^{-6} \times A_T\right) + 7.01 \times 10^{-4} \qquad (5)$$

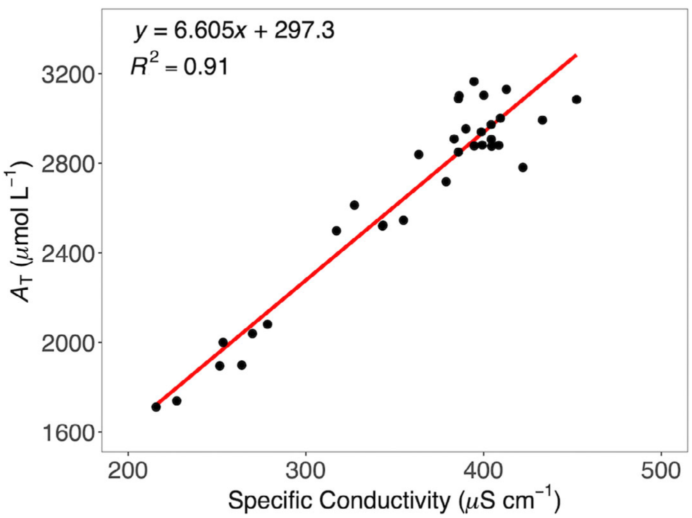

Fig. 1. The relationship between A_T and specific conductivity obtained on the CFR at GC used to calculate A_T for pCO_2 computation. The red line is the linear best fit ($n = 33$). The average residual A_T is 0 ± 130 μmol L^{-1}.

The Bearmouth sampling site is located on the CFR (46°42′16″N, 113°20′41″W) ~55 km downstream of the deployment site and has similar chemical composition (i.e., pH and A_T; Nagorski 2001). To obtain Eq. 5, ionic strength was calculated from Eq. 4 from measured total ion concentrations (HCO_3^-, Ca^{2+}, K^+, Mg^{2+}, Na^+, SO_4^{2-}, SiO_3^{2-}) in surface water samples and linearly correlated with A_T (Nagorski 2001). Equation 5 was then used to estimate μ during the deployment using the conductivity-derived A_T from Fig. 1.

Data analysis

The primary statistical analyses used for this study were linear regression analysis and Student's T-test ($\alpha = 0.05$). These tools allowed us to examine the significance of direct comparisons between pH measurements as well as calculated pCO_2 values. Graphical visualization techniques, which include error and 1 : 1 plots, were also used to explore dataset-wide trends as they related to differences in pH measurements and pCO_2 values.

Assessment

Laboratory study

Electrochemical and spectrophotometric pH comparisons

The tank experiment took place over a 7-month period where 35 tank samples were analyzed for pH and A_T. The overall measured pH_{NBS} in the test tank ranged from 7.91 to 9.11 with an average pH of 8.40 ± 0.29. The standard deviation of the spectrophotometric pH replicates ranged from ± 0.0001 to ± 0.02 pH units ($n = 3$) over the range of pCO_2 in the test tank (~100–1600 μatm). During the study, no

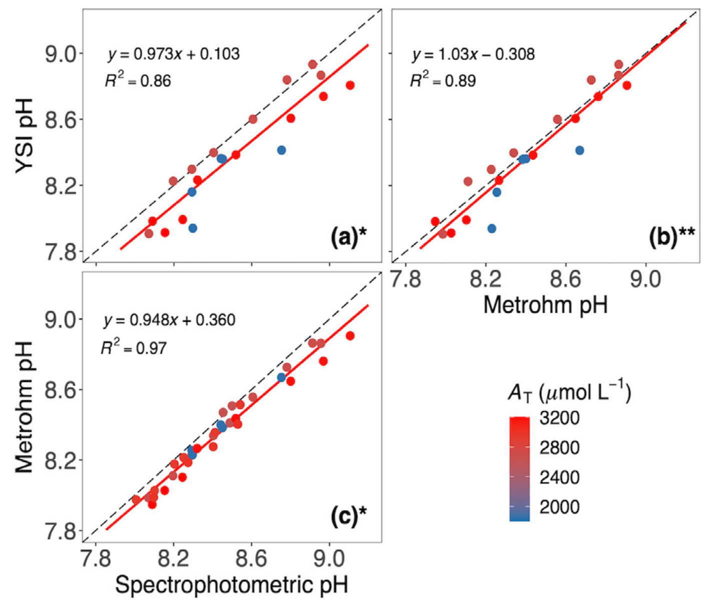

Fig. 2. A comparison of in situ electrochemical and spectrophotometric pH_{NBS} measured in the test tank (15.2 ± 2.2°C). The pH was varied by changing the pCO_2 and A_T (see "Methods" section). (**a**) YSI pH electrode vs. spectrophotometric pH data. (**b**) YSI pH electrode vs. the Metrohm pH electrode data. (**c**) Metrohm pH electrode vs. spectrophotometric pH data. Data points are colored by measured A_T in the test tank and range from 1841 to 3195 μmol L^{-1}. The 1 : 1 line (black dashed line) and linear regression (red line) are also shown with the equation and the R^2 in the upper left of each plot. The symbols * and ** indicate that the x- and y-axis variables are statistically different ($p < 0.05$) or not ($p > 0.05$), respectively. Error bars for the spectrophotometric pH values have been omitted because the range of the error is too small to be seen on the x-axis range (0.00017–0.016 pH units).

Table 1. The average ($\pm$ SD) differences for each regression analysis and R^2 values for the three pH techniques of spectrophotometric (Spec), Metrohm, and YSI found in Fig. 2. The symbols * or ** indicate that the comparison is either statistically different or not, respectively, with an $\alpha = 0.05$.

Average differences ($\pm$ SD)	Spec—Metrohm* ($n = 35$)	0.084 ± 0.050	$R^2 = 0.97$
	Spec—YSI* ($n = 21$)	0.13 ± 0.12	$R^2 = 0.86$
	Metrohm—YSI** ($n = 21$)	0.036 ± 0.11	$R^2 = 0.89$

replicate samples were taken for electrochemical pH measurements (i.e., Metrohm and YSI). However, an independent assessment of the precision of each electrode found the Metrohm ($n = 6$) and YSI ($n = 6$) pH precisions to be ± 0.005 and ± 0.05 pH units, respectively. Note that the digital resolution of the Metrohm and YSI pH meters are ± 0.001 and 0.01, respectively.

Fig. 2 shows that spectrophotometric pH_{NBS} and electrochemical pH_{NBS} data fall below the 1 : 1 line indicating that

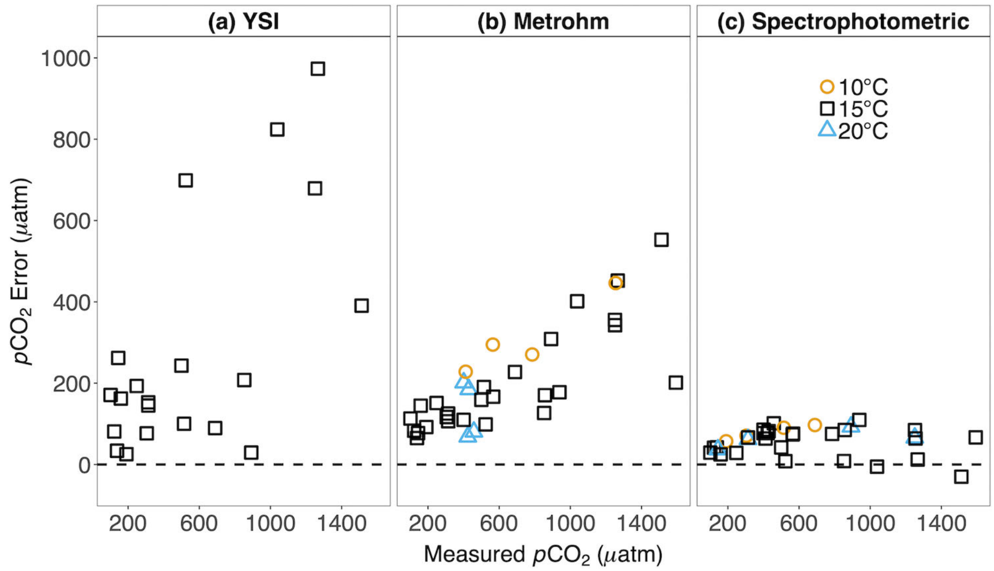

Fig. 3. The pCO_2 error (calculated − measured) vs. measured pCO_2. Spectrophotometric ($n = 34$), Metrohm ($n = 34$), and YSI ($n = 20$) pH_{NBS} data are used to calculate pCO_2 using the equilibrium program CO2SYS at infinite dilution. The dashed black line represents zero error. Measured A_T values ranged from 1841 to 3195 μmol L^{-1}. Different symbols represent different in situ tank temperatures. Calculated pCO_2 from the (**b**) Metrohm and (**c**) spectrophotometric pH measurements were analyzed at 10°C ($n = 4$), 15°C ($n = 26$), and 20°C ($n = 4$), whereas calculated pCO_2 from the (**a**) YSI pH electrode was only analyzed at 15°C ($n = 20$).

both electrode pH data are lower than the corresponding spectrophotometric pH measurements ($p < 0.001$; Table 1). The pH electrode data are uniformly scattered around the 1 : 1 line (Fig. 2b) and there is no statistical difference between the two electrochemical pH datasets ($p > 0.05$; Table 1; Fig. 2b). In addition, the slopes derived from the linear regressions between spectrophotometric and electrochemical pH are statistically different from 1.0 (Fig. 2a,c; $p < 0.001$). The slopes < 1.0 appear to arise from systematically larger pH differences at higher pH (i.e., pH > 8.7; Fig. 2a,c).

The coefficients of determination (R^2) for each pH comparison were found to be 0.86, 0.89, and 0.97 for Fig. 2a–c, respectively (Table 1). These values further illustrate differences in random errors between the electrochemical and spectrophotometric pH measurements. The lower R^2 values appear to be due to larger random errors from the YSI pH electrode (Table 1; Fig. 2a,b) reflecting the replicate precision discussed above. The standard deviation of the residuals for each regression analysis was ± 0.12, ± 0.11, and ± 0.05 pH units (Fig. 2a–c, respectively), with the larger residual standard deviations corresponding to the regressions involving the YSI pH electrode.

Calculated pCO_2

The pCO_2 errors calculated from the pH_{NBS} data in Fig. 2 were assessed over a pCO_2 range of 101–1593 μatm. The pCO_2 was calculated using CO2SYS at infinite dilution, discussed above, to be able to focus solely on how pH measurements affect calculated pCO_2. Later, a thermodynamically rigorous

Table 2. The average (± SD) and range of calculated pCO_2 and pCO_2 error (compared to the measured pCO_2) between the three pH techniques calculated from CO2SYS at infinite dilution. The average percent error of each pH technique relative to the measured pCO_2 is also reported.

		Spectrophotometric ($n = 34$)	Metrohm ($n = 34$)	YSI ($n = 20$)
Calculated pCO_2 (μatm)	Average (± SD)	683 ± 417	825 ± 522	826 ± 643
	Range	130–1660	203–2065	172–2240
pCO_2 error (μatm)	Average (± SD)	58 ± 33	203 ± 125	277 ± 284
	Range	−30 to 110	65–553	25–973
Percent error (%)	Average (± SD)	14 ± 9	40 ± 21	62 ± 51

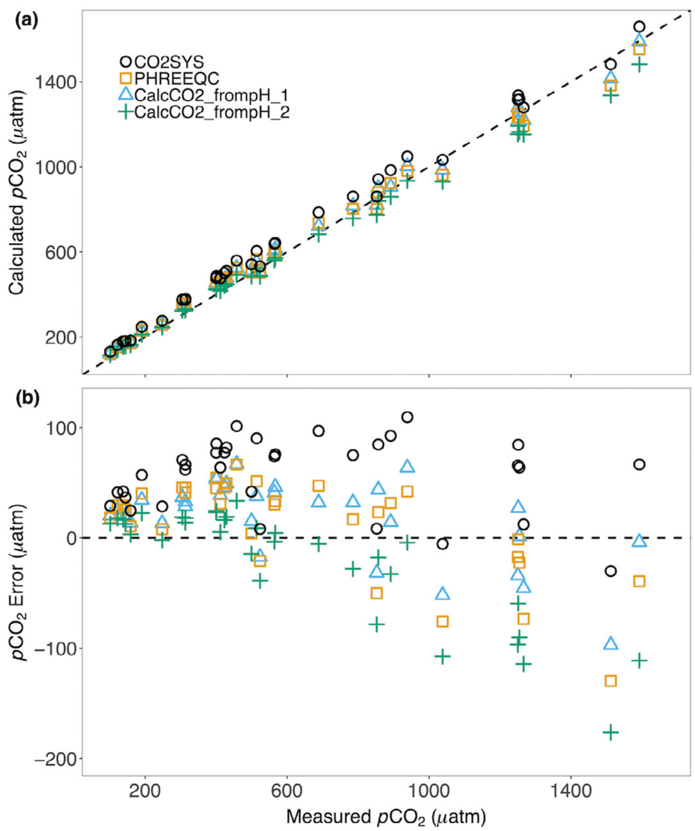

Fig. 4. (**a**) The comparison of pCO_2 calculated from spectrophotometric pH and A_T using different equilibrium models to measured pCO_2. The dashed black line represents the 1 : 1 line. pH_{free} and pH_{NBS} were used to be consistent with the pH scales in each program. (**b**) The pCO_2 error (calculated − measured) vs. measured pCO_2 ($n = 136$). The black dashed line represents zero error.

comparison is made to illustrate deviations in calculated pCO_2 due to μ. The pCO_2 error dependence on pCO_2 levels is shown in Fig. 3. The error in calculated pCO_2 using the Metrohm and YSI pH electrodes generally increased with increasing pCO_2 (Fig. 3a,b), whereas the error in calculated pCO_2 from spectrophotometric pH appears relatively consistent with increasing pCO_2 (Fig. 3c). Spectrophotometric, Metrohm, and YSI pH had average pCO_2 errors (calculated – measured) of 58 ± 33, 203 ± 125, and 277 ± 284 μatm, respectively (Table 2). In addition, the average percent errors from spectrophotometric, Metrohm, and YSI pH are $14\% \pm 9\%$, $40\% \pm 21\%$, and $62\% \pm 51\%$, respectively (Table 2). Metrohm and YSI calculated pCO_2 also displayed the largest absolute errors of 553 and 973 μatm, respectively (Table 2). Furthermore, temperature did not appear to affect pCO_2 error regardless of the pH used (Fig. 3b,c). The systematically high pCO_2 values from the electrode measurements (Fig. 3a,b; Table 2) supports that the pH bias shown in Fig. 2 is due to errors in the electrode pH. The precision of calculated pCO_2 among the three pH techniques was also assessed. The pCO_2 precision from the two pH electrodes was $\pm$ 125 and $\pm$ 284 for Metrohm and YSI pH, respectively; compared to $\pm$ 33 μatm for spectrophotometric pH (Table 2; SD of pCO_2 errors). From Fig. 3 data, it is evident that pCO_2 calculated using spectrophotometric pH is both more accurate and precise compared to pCO_2 calculated from electrochemical pH (Fig. 3c; Table 2), especially at higher pCO_2 levels.

It is important to mention, here, that the tank DOC ranged from ~ 8 to 42 μmol L^{-1} ($n = 6$) during the study. Following the conclusions in Liu et al. (2020), that states that in more alkaline waters (e.g., pH = 7–8.5 and $A_T > 1000$ μmol L^{-1}) low in DOC (e.g., < 350 μmol L^{-1}) the contribution of "excess A_T" from organic acid anions is negligible. Therefore, the tank water DOC was assumed to be too low to significantly contribute to the measured A_T, and consequently, the calculated pCO_2.

Assessment of μ *and associated* pCO_2 *error*

The importance of μ was initially underestimated in our pCO_2 accuracy evaluations as μ in freshwater systems is typically assumed to be zero (Hunt et al. 2011; Stets et al. 2017). We noticed that the calculated pCO_2 error would change depending on (1) the μ used to calculate in situ pH (Eqs. 1, 3) and (2) if μ was used to calculate apparent equilibrium constants (i.e., K'_1, K'_2, and K'_H). This led to the μ sensitivity tests using four different programs, CO2SYS at infinite dilution, PHREEQC, CalcCO2_frompH_1, and CalcCO2_frompH_2, which illustrate different approaches for using μ (Fig. 4;

Table 3. The average ($\pm$ SD) pCO_2 error (|calculated − measured pCO_2|) and range using different μ in CO2SYS (infinite dilution), PHREEQC, and CalcCO2_frompH. CalcCO2_frompH_1 and CalcCO2_frompH_2 use μ calculated from AWQR (2020) and Griffin and Jurinak (1973), respectively. μ averages ($\pm$ SD) are included in the header and represent the μ used to calculate the apparent dissociation constants. Averages were taken from absolute values to avoid biases from large positive and negative values. The range is not reported in absolute values to illustrate the true range of pCO_2 error.

	CO2SYS ($n = 34$) $\mu = 0$ mM	**PHREEQC ($n = 34$) $\mu = 2.8 \pm 0.4$ mM**	**CalcCO2_frompH_1 ($n = 34$) $\mu = 7.4 \pm 1.2$ mM**	**CalcCO2_frompH_2 ($n = 34$) $\mu = 4.2 \pm 0.7$ mM**
Average ($\pm$ SD)	58 ± 29	38 ± 24	35 ± 19	37 ± 42
Range	−30 to 110	−130 to 67	−97 to 67	−176 to 34

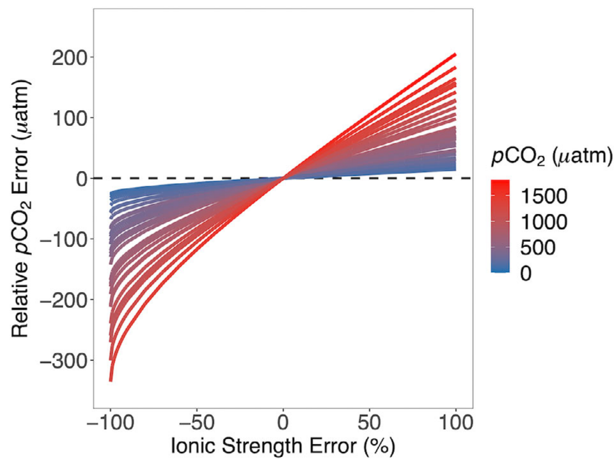

Fig. 5. Modeled relative pCO_2 error for percent error in μ where individual lines are colored by calculated pCO_2 (μatm). Only the spectrophotometric pH_{free} dataset was used for this model, thus, the pCO_2 calculated from spectrophotometric pH_{free} lies at 0% ionic strength error and zero pCO_2 error. The black dashed line represents zero calculated pCO_2 error. All model calculations of pCO_2 were done using the CalcCO2_frompH script at in situ tank temperatures.

Table 3). CalcCO2_frompH_1 and CalcCO2_frompH_2 pCO_2 values were calculated using spectrophotometric pH and A_T with calculated μ from the Missoula Aquifer (AWQR 2020) and from the Griffin and Jurinak (1973) relationship, respectively. The relationship from Griffin and Jurinak (1973) correlates μ with conductivity, but it is derived from soil water and river samples, making its comparison to CalcCO2_frompH_1 useful for broadscale applicability in other systems. Spectrophotometric pH_{free} measurements were used in CalcCO2_frompH_1 and CalcCO2_frompH_2. To be consistent with the pH scales, spectrophotometric pH_{NBS} values were used in both CO2SYS (infinite dilution) and PHREEQC. pCO_2 values calculated with CO2SYS were included to be able to compare to how pCO_2 is conventionally calculated in the literature and are the same values presented in Fig. 3c. In addition, PHREEQC calculates μ within its program from the input A_T (i.e., $[HCO_3^-]$) and counterion used to achieve charge balance (e.g., $[Na^+]$), neglecting other ions potentially present in waters. Thus, the μ used for the apparent dissociation constants are lower in PHREEQC compared to CalcCO2_frompH_1 and CalcCO2_frompH_2 (Table 3). Furthermore, the average and standard deviation of μ presented in Table 3 reflect the differences in the approaches used for estimating μ. Different approaches explicitly assume different ionic species concentration.

The different calculated pCO_2 values are compared to the measured pCO_2 using a 1 : 1 plot (Fig. 4a) where most values appear to follow the 1 : 1 line with minimal spread. However, when looking at the pCO_2 error, a "fanning-out" pattern becomes clear as you go from low to high pCO_2 levels (Fig. 4b). The pCO_2 calculated from CO2SYS at infinite dilution generally overestimated pCO_2 while the pCO_2 calculated using apparent dissociation constants (CalcCO2_frompH and PHREEQC) generally underestimated pCO_2 at higher levels (Fig. 4b). Compared to the average error from PHREEQC, CalcCO2_frompH_1, and CalcCO2_frompH_2, the average error calculated from CO2SYS is significantly larger ($p < 0.01$; Table 3). The average error from PHREEQC, CalcCO2_frompH_1, and CalcCO2_frompH_2 is not significantly different from each other ($p > 0.05$; Table 3). Recall that CO2SYS and CalcCO2_frompH use the same equilibrium constants; thus, at infinite dilution these two programs calculate the same pCO_2 values when using the same pH scale. The differences in calculated pCO_2 between CO2SYS and CalcCO2_frompH arise in part because of the differences between pH_{NBS} and pH_{free} (Eq. 3). The error in calculated pCO_2 gets further compounded by differences in infinite dilution dissociation constants (i.e., CO2SYS) and apparent dissociation constants (i.e., CalcCO2_frompH). Moreover, we see an increase in calculated pCO_2 with increasing μ using pH_{free} and CalcCO2_frompH as noted by the decreasing error from CalcCO2_frompH_2 to CalcCO2_frompH_1 (Fig. 4b). The increase in calculated pCO_2 from higher μ is a result of the covariation between pH_{free} and the apparent dissociation constants within CalcCO2_frompH. Conversely, we see a decrease in calculated pCO_2 with higher μ using pH_{NBS} (CO2SYS compared to PHREEQC; Fig. 4b; Table 3).

To further evaluate μ effects on calculated pCO_2 error, the pCO_2 error was modeled as a function of μ percent error. The pCO_2 calculated from spectrophotometric pH_{free} and its associated μ (calculated from AWQR 2020) were used as the reference dataset (dataset in Fig. 4; CalcCO2_frompH_1). The reference spectrophotometric pH_{free} values were adjusted by using the Davies term (right side of Eq. 3) to account for the modeled μ percent error. Fig. 5 illustrates the range for calculated pCO_2 error from zero ionic strength (e.g., −100% ionic strength error) to double the reference ionic strength (e.g., +100% ionic strength error; μ = 14.8 mM) over the range of pCO_2 found during the tank study. The relative error is also a function of pCO_2 where high pCO_2 error is associated with high pCO_2 levels and large μ error (Fig. 5). Furthermore, if μ is assumed to be zero (i.e., −100% ionic strength error) as is commonly done in freshwater CO_2 studies (Stets et al. 2017), the uncertainty in calculated pCO_2 error is ~ 20%. Moreover, at a − 50% μ error relative to CalcCO2_frompH_1 (i.e., CalcCO2_frompH_2; Table 3), the average modeled pCO_2 error (from absolute values) was not statistically different from the CalcCO2_frompH_2 error (Table 3; $p > 0.05$).

Field application

The time series from the field study are shown in Fig. 6. Riverine pH_{free} and temperature measured from the SAMI-pH during the deployment ranged from 8.11 to 8.83 (average of 8.41 ± 0.21) and 1.7°C to 21.3°C (average of 12.7°C ± 4.6°C), respectively (Fig. 6a,b). Conductivity-derived A_T (Fig. 6c), specific conductivity (Supporting Information Fig. S2a), and μ

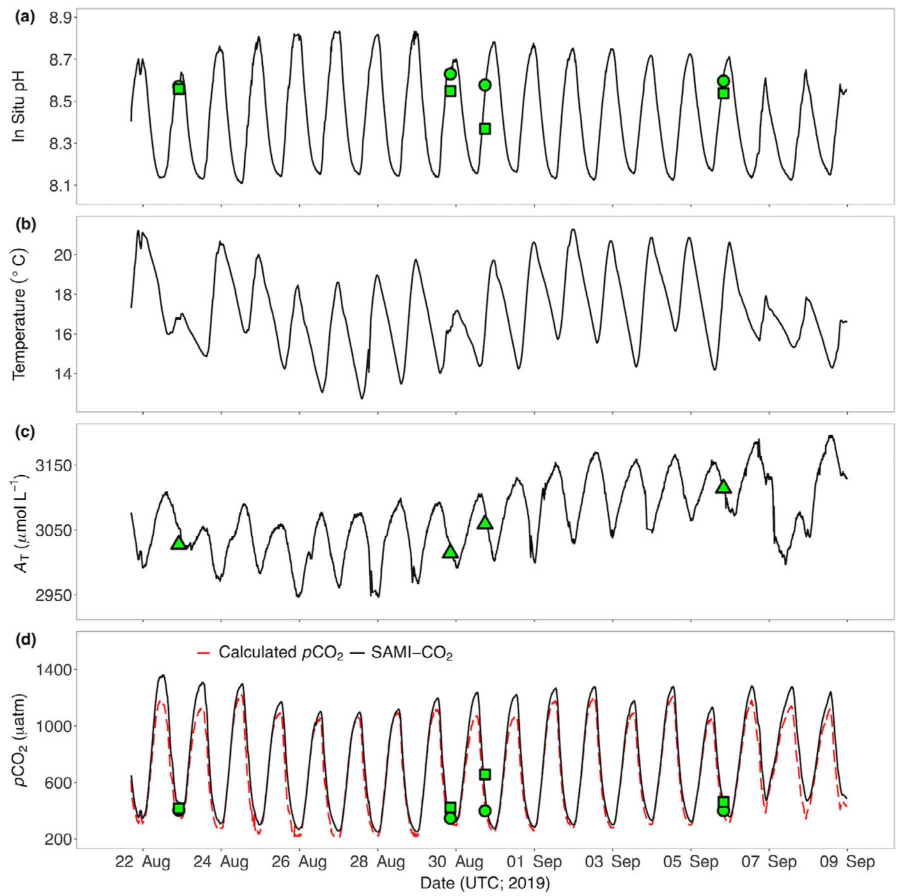

Fig. 6. A 19-d in situ time series from the CFR of (**a**) spectrophotometric pH_{free}, (**b**) temperature, (**c**) conductivity-derived A_T, and (**d**) measured pCO_2 (SAMI-CO_2; solid black line) and calculated pCO_2 (SAMI-pH and conductivity-derived A_T; red dashed line). Discrete samples of measured pH and calculated pCO_2 using spectrophotometric pH (green circles) and YSI pH (green squares) are also shown in (**a**) and (**d**), respectively. Discrete A_T samples are represented by green triangles in (**c**). The date and time displayed is UTC during the year 2019.

(Supporting Information Fig. S2b) ranged from 2490 to 3440 μmol L^{-1} (average $= 3050 \pm 113$ μmol L^{-1}), 394.4 to 465.4 μS cm^{-1} (average $= 424.4 \pm 8.7$ μS cm^{-1}), and 7.3 to 9.7 mM (average $= 8.7 \pm 0.3$ mM), respectively. The average diel range of pH was ~ 0.6 pH units and the average diel range of pCO_2 was ~ 900 μatm (Fig. 6a,d). The average difference between discrete pH and SAMI-pH measurements was -0.003 ± 0.028 pH units for spectrophotometric pH and -0.09 ± 0.06 pH units for YSI pH. The average difference between discrete A_T and conductivity-derived A_T was -14 ± 11 μmol L^{-1}. Furthermore, the pCO_2 calculated from spectrophotometric and YSI pH discrete samples had average differences of -66 ± 39 and 35 ± 71 μatm, respectively, when compared to SAMI-CO_2 measurements (Fig. 6d).

The in situ pH_{free} (Fig. 6a; Eq. 1) data was used with conductivity-derived A_T (Fig. 1 and Fig. 6c), μ (Supporting Information Fig. S2b; Eq. 5) and temperature (Fig. 6b) to calculate pCO_2 (Fig. 6d). The average difference between the calculated and measured pCO_2 is -70 ± 57 μatm with an average percent error of $10\% \pm 7\%$ (Fig. 7). We found that the error in calculated pCO_2 during the field application was pCO_2 dependent, for example, the average error was -55 ± 52 μatm at $pCO_2 < 1000$ μatm and -102 ± 55 μatm at $pCO_2 > 1000$ μatm (Fig. 7b). This error can be partially explained by uncertainty in the conductivity-derived A_T where the residual uncertainty from the Fig. 1 linear fit is ± 130 μmol L^{-1}. It is important to note that the uncertainty of the A_T (Supporting Information Fig. S1) and specific conductivity (< 5 μS cm^{-1}) measurements are much less than the uncertainty reported by the linear least-squares regression (Fig. 1). This suggests that the scatter of this relationship is caused by biogeochemical factors and not measurement error. Instead, this relatively large uncertainty could be driven by evapotranspiration (ET) which creates diel inputs of groundwater (Dodds et al. 2017; Shangguan et al. 2021). In addition, there appears to be a repeating clockwise pattern in pCO_2 error (i.e., hysteresis) (Fig. 7b). Further discussion of potential mechanisms that may explain this pattern are provided below.

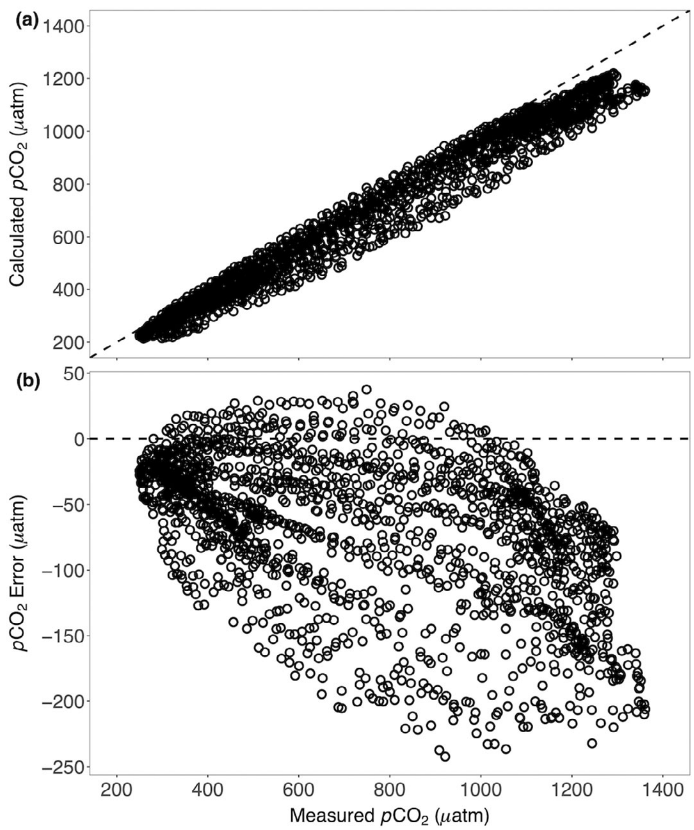

Fig. 7. (**a**) The comparison of measured pCO_2 and pCO_2 calculated from SAMI-pH and conductivity-derived A_T during the in situ deployment in the CFR. The dashed black line represents the 1 : 1 line. (**b**) The pCO_2 error (calculated − measured) vs. measured pCO_2 ($n = 1685$). The dashed black line represents zero error. See Fig. 6c for the conductivity-derived A_T value range during the deployment. The CalcCO2_frompH script with μ estimated from Eq. 5 was used to calculated pCO_2.

Discussion

It is evident in Figs. 2, 3, Tables 1, 2, and the statistics stated in the *Assessment* that spectrophotometric pH has significantly better replicate precision than electrochemical pH and, based on its application for calculation of pCO_2, significantly better accuracy. Spectrophotometric pH is based on highly reproducible and accurate optical absorbances in contrast to the pH electrode potential that is affected by many environmental and instrumental factors (e.g., ionic strength gradient, buffer composition, reference potential, etc.). The conclusions presented here support findings of past studies that electrode pH is systematically low in low ionic strength solutions (Illingworth 1981; Herczeg and Hesslein 1984; Davison and Woof 1985) stemming from the liquid junction of the reference electrode.

The spectrophotometric pH accuracy and precision translates into greatly improved estimation of pCO_2 from pH and A_T. The large differences in pCO_2 calculated from the two pH electrodes show that, while electrode performance might be adequate under some circumstances, it is difficult to control and predict even in a controlled laboratory study with carefully calibrated electrodes.

This study also found that accounting for μ in the equilibrium constants and pH_{free} can improve calculated pCO_2 accuracy (Fig. 4). The pCO_2 error is reduced using the best available μ (Table 3, CalcCO2_frompH_1) compared to the common practice of using CO2SYS at infinite dilution (Table 3). Furthermore, theoretical calculations indicate that changes in μ can alter equilibrium constants and impact calculated pCO_2 (Fig. 5). Moreover, theoretical calculations (Fig. 5) were also able to predict a similar average error that was observed for CalcCO2_frompH_2.

The average percent error in calculated pCO_2 from spectrophotometric pH_{free} (using CalcCO2_frompH) from the tank study and field application is 8% ± 6% and 10% ± 7%, respectively. The field application using in situ sensors demonstrated that spectrophotometric pH can be employed in a real-world application and produce similar results found in a controlled laboratory setting. As discussed above, the error in calculated pCO_2 during the field application was pCO_2 dependent (Figs. 6, 7). Errors were largest at high pCO_2 levels which occurred at night due to respiration (Figs. 6d, 7). Furthermore, error in the conductivity-derived A_T relationship likely contributed significantly to the observed pCO_2 error from the field application. As discussed above, the residual uncertainty in the relationship between specific conductivity and A_T (Fig. 1) ranged from −303 to 262 μmol L^{-1} with a standard deviation of ± 130 μmol L^{-1}. The large residuals are mostly driven by the data with high specific conductivity and high A_T (Fig. 1), measurements that are common during base flow conditions. Because the field study took place during base flow conditions, uncertainties in the conductivity-derived A_T time series could contribute to the observed differences between calculated and measured pCO_2 (Figs. 6d; Supporting Information Fig. S3). To examine this idea, the standard deviation of residuals (± 130 μmol L^{-1}) was added to and subtracted from the entire conductivity-derived A_T time series (Fig. 6c) to create upper and lower bounds (Supporting Information Fig. S3). These limits were then used to calculate pCO_2, as described previously. Supporting Information Fig. S3 reveals that for most of the diel cycles, error in the conductivity-derived A_T can explain a significant part of the difference between calculated and measured pCO_2, where the original calculated pCO_2 error (Fig. 6d) is significantly different from the uncertainty corrected pCO_2 error (Supporting Information Fig. S3, upper orange ribbon boundary) ($p < 0.001$). The average pCO_2 error and percent error were reduced to −34 ± 54 μatm ($n = 1685$) and 7% ± 6%, respectively, a 51% improvement in calculated pCO_2 error. As discussed above, ET can drive A_T and conductivity diel cycles (Wilcock and Chapra 2005; Shangguan et al. 2021) and is likely controlling the diel A_T in the CFR (Shangguan et al. 2021), with lower groundwater signals during the day (lower A_T) due to riparian groundwater uptake.

Thus, ET accounts for the major uncertainty of the A_T–conductivity relationship during base flow (Fig. 1). This proposed mechanism seems to explain most of the difference between the calculated and measured pCO$_2$ during the field application portion of this study (Fig. 6; Supporting Information Fig. S3). In addition, the error in calculated pCO$_2$ may be further attributed to photo-contamination and/or temperature effects within the pH and pCO$_2$ sensors. Figure 7b indicates a cyclic pattern between pCO$_2$ error and measured pCO$_2$. Upon further exploration, we found that this hysteresis pattern is driven by a diel signal (i.e., solar radiation, temperature) in the river that causes the sensor's blank intensities to change. We believe, however, that this error is minor compared to the conductivity-derived A_T uncertainty.

Lastly, accurate pCO$_2$ is critical for constraining air–water fluxes. Therefore, the observed percent uncertainty in computed pCO$_2$ (8% ± 6%) from spectrophotometric pH$_{free}$, A_T, and μ (see dataset in Fig. 4; CalcCO2_frompH_1) presented in this study would translate to a similar percent uncertainty when estimating CO$_2$ gas fluxes. Thus, more accurate CO$_2$ gas flux estimates could be obtained from spectrophotometric pH than from electrochemical pH, which had an observed percent uncertainty in computed pCO$_2$ of > 40% (Table 2).

Comments and recommendations

The study clearly demonstrates the advantages of using spectrophotometric pH for freshwater pCO$_2$ calculations. pH is of course a master variable in aquatic systems and a wide array of freshwater research could potentially benefit from higher quality pH measurements. Spectrophotometric pH data might improve model calculations of metal speciation/complexation and toxicity modeling (Wang et al. 2016; Huang et al. 2017), calcium carbonate saturation (Müller et al. 2015; Khan et al. 2021), and net ecosystem production (Oren et al. 2006; Lynch et al. 2010; Kanuri et al. 2017). Highly reproducible pH measurements will also be valuable for monitoring long-term changes in pH due to CO$_2$ acidification or other long-term anthropogenic impacts in rivers and lakes (Butman and Raymond 2011; Phillips et al. 2015; Arroita et al. 2019; Minor et al. 2019). Moreover, a "do-it-yourself" portable photometer developed for seawater (Yang et al. 2014; Wang et al. 2019), could make discrete freshwater measurements of spectrophotometric pH for the computation of pCO$_2$ easier in the field. It remains, however, that measuring freshwater pCO$_2$ directly rather than computing it from inorganic carbon parameters is preferred, as is true for seawater. Although, our focus is on riverine CO$_2$, these findings and subsequent conclusions apply to all freshwater systems.

Future experiments should expand the pCO$_2$ range to include much higher levels (e.g., 2000–10,000 μatm), vary the temperature over a larger range (0–30°C), and evaluate at lower A_T (e.g., < 1000 μmol L^{-1}; Liu et al. 2020). Organic acid concentrations could further increase pCO$_2$ error and should also be considered in future studies with spectrophotometric pH and A_T. An additional complicating factor with spectrophotometric pH is that colored dissolved organic matter could cause inaccurate absorbance readings at high concentrations and could therefore lead to inaccurate pH values (i.e., tenths of pH units too low in strongly colored waters, Müller et al. 2017). This might mostly be corrected by the blank but needs to be tested, nonetheless. Thus, at high DOC concentrations both A_T and spectrophotometric pH measurements could be biased. The findings from this study also indicate that inaccurate μ contributes significantly to calculated pCO$_2$ uncertainty and must be accounted for to minimize pCO$_2$ error. In addition, a caveat to our conclusions regarding field measurements of spectrophotometric pH is that the CFR is a well buffered system and so the indicator pH perturbation is relatively small (as discussed in "Methods" section). This perturbation effect could be larger in other, less buffered systems (<1000 μmol L^{-1}) even if they are corrected using established methods (Yuan and DeGrandpre 2008; Lai et al. 2016).

References

Åberg, J., and M. Wallin. 2014. Evaluating a fast headspace method for measuring DIC and subsequent calculation of pCO$_2$ in freshwater systems. Inland Waters **4**: 157–166. doi:10.5268/iw-4.2.694

Abril, G., and others. 2014. Amazon River carbon dioxide outgassing fueled by wetlands. Nature **505**: 395–398. doi:10.1038/nature12797

Abril, G., and others. 2015. Technical note: Large overestimation of pCO$_2$ calculated from pH and alkalinity in acidic, organic-rich freshwaters. Biogeosciences **12**: 67–78. doi:10.5194/bg-12-67-2015

Aho, K. S., J. D. Hosen, L. A. Logozzo, W. R. McGillis, and P. A. Raymond. 2021. Highest rates of gross primary productivity maintained despite CO$_2$ depletion in a temperate river network. Limnol. Oceanogr. Lett. **6**: 200–206. doi:10.1002/lol2.10195

Annual Water Quality Report (AWQR). 2020. 2020 Annual water quality report. Missoula (MT): City of Missoula. Available from: https://www.ci.missoula.mt.us/DocumentCenter/View/52629/2020-CCR—Missoula-Water?bidId=

Appling, A. P., R. O. Hall, C. B. Yackulic, and M. Arroita. 2018a. Overcoming equifinality: Leveraging long time series for stream metabolism estimation. J. Geophys. Res. Biogeo. **123**: 624–645. doi:10.1002/2017jg004140

Appling, A. P., J. S. Read, L. A. Winslow, M. Arroita, E. S. Bernhardt, N. A. Griffiths, R. O. Hall Jr., J. W. Harvey, J. B. Heffernan, E. H. Stanley, E. G. Stets, and C. B. Yackulic. 2018b. The metabolic regimes of 356 rivers in the United States. Sci. Data **5**: 180–292. doi:10.1038/sdata.2018.292

Arroita, M., A. Elosegi, and R. O. Hall. 2019. Twenty years of daily metabolism show riverine recovery following sewage abatement. Limnol. Oceanogr. **64**: 77–92. doi:10.1002/lno.11053

Aufdenkampe, A. K., E. Mayorga, P. A. Raymond, J. M. Melack, S. C. Doney, S. R. Alin, R. E. Aalto, and K. Yoo. 2011. Riverine coupling of biogeochemical cycles between land, oceans, and atmosphere. Front. Ecol. Environ. **9**: 53–60. doi:10.1890/100014

Ball, J. W., and D. K. Nordstrom. 1991. WATEQ4F—User's manual with revised thermodynamic data base and test cases for calculating speciation of major, trace and redox elements in natural waters. Open-file report. U.S. Geological Survey. doi:10.3133/ofr90129

Barnes, I. 1964. Field measurement of alkalinity and pH. Geochemistry of Water: Geological Survey Water-Supply Paper. U.S. Geological Survey **1535-H**: 1–17. doi:10.3133/wsp1535h

Bockmon, E. E., and A. G. Dickson. 2015. An inter-laboratory comparison assessing the quality of seawater carbon dioxide measurements. Mar. Chem. **171**: 36–43. doi:10.1016/j.marchem.2015.02.002

Butman, D., and P. A. Raymond. 2011. Significant efflux of carbon dioxide from streams and rivers in the United States. Nat. Geosci. **4**: 839–842. doi:10.1038/ngeo1294

Byrne, R. H., G. Robert-Baldo, S. W. Thompson, and C. T. A. Chen. 1988. Seawater pH measurements: An at-sea comparison of spectrophotometric and potentiometric methods. Deep Sea Res. Part A Oceanogr. Res. Pap. **35**: 1405–1410. doi:10.1016/0198-0149(88)90091-x

Byrne, R. H., S. Mecking, R. A. Feely, and X. Liu. 2010. Direct observations of basin-wide acidification of the North Pacific Ocean. Geophys. Res. Lett. **37**: 1–5. doi:10.1029/2009gl040999

Chen, C.-T. A., T.-H. Huang, Y.-H. Fu, Y. Bai, and X. He. 2012. Strong sources of CO_2 in upper estuaries become sinks of CO_2 in large river plumes. Curr. Opin. Environ. Sustain. **4**: 179–185. doi:10.1016/j.cosust.2012.02.003

Choi, J., S. M. Hulseapple, M. H. Conklin, and J. W. Harvey. 1998. Modeling CO_2 degassing and pH in a stream–aquifer system. J. Hydrol. **209**: 297–310. doi:10.1016/s0022-1694(98)00093-6

Cole, J. J., and N. F. Caraco. 2001. Carbon in catchments: Connecting terrestrial carbon losses with aquatic metabolism. Mar. Freshw. Res. **52**: 101. doi:10.1071/mf00084

Cole, J. J., and others. 2007. Plumbing the global carbon cycle: Integrating inland waters into the terrestrial carbon budget. Ecosystems **10**: 172–185. doi:10.1007/s10021-006-9013-8

Coles, J. F., Riva-Murray, K., Van Metre, P. C., Button, D. T., Bell, A. H., Qi, S. L., Journey, C. A., and Sheibley, R. W. 2019. Design and methods of the U.S. Geological Survey Northeast Stream Quality Assessment (NESQA): Open-File Report 2018–1183. U.S. Geological Survey. 46 p. https://doi.org/10.3133/ofr20181183.

Cormier, S. M., S. P. Wilkes, and L. Zheng. 2013. Relationship of land use and elevated ionic strength in Appalachian watersheds. Environ. Toxicol. Chem. **32**: 296–303. doi:10.1002/etc.2055

Davison, W., and C. Woof. 1985. Performance tests for the measurement of pH with glass electrodes in low ionic strength solutions including natural waters. Anal. Chem. **57**: 2567–2570. doi:10.1021/ac00290a031

DeGrandpre, M. D., T. R. Hammar, S. P. Smith, and F. L. Sayles. 1995. In situ measurements of seawater pCO_2. Limnol. Oceanogr. **40**: 969–975. doi:10.4319/lo.1995.40.5.0969

DeGrandpre, M. D., R. S. Spaulding, J. O. Newton, E. J. Jaqueth, S. E. Hamblock, A. A. Umansky, and K. E. Harris. 2014. Considerations for the measurement of spectrophotometric pH for ocean acidification and other studies. Limnol. Oceanogr. Methods **12**: 830–839. doi:10.4319/lom.2014.12.830

DeGrandpre, M. D., C. Z. Lai, M. L. Timmermans, R. A. Krishfield, A. Proshutinsky, and D. Torres. 2019. Inorganic carbon and pCO_2 variability during ice formation in the Beaufort Gyre of the Canada Basin. J. Geophys. Res. Oceans **124**: 4017–4028. doi:10.1029/2019jc015109

Dickson, A. G., C. L. Sabine, and J. R. Christian. 2007. Guide to best practices for ocean CO_2 measurements. North Pacific Marine Science Organization.

Dodds, W. K., F. Tromboni, W. Aparecido Saltarelli, and D. G. Fernandes Cunha. 2017. The root of the problem: Direct influence of riparian vegetation on estimation of stream ecosystem metabolic rates. Limnol. Oceanogr. Lett. **2**: 9–17. doi:10.1002/lol2.10032

Duvert, C., D. E. Butman, A. Marx, O. Ribolzi, and L. B. Hutley. 2018. CO_2 evasion along streams driven by groundwater inputs and geomorphic controls. Nat. Geosci. **11**: 813–818. doi:10.1038/s41561-018-0245-y

French, C. R., J. J. Carr, E. M. Dougherty, L. A. K. Eidson, J. C. Reynolds, and M. D. DeGrandpre. 2002. Spectrophotometric pH measurements of freshwater. Anal. Chim. Acta **453**: 13–20. doi:10.1016/s0003-2670(01)01509-4

Gran, G. 1952. Determination of the equivalence point in potentiometric titrations. Part II. Analyst **77**: 661. doi:10.1039/an9527700661

Gray, S. E., M. D. DeGrandpre, C. Langdon, and J. E. Corredor. 2012. Short-term and seasonal pH, pCO_2 and saturation state variability in a coral-reef ecosystem. Global Biogeochem. Cycl. **26**: 1–13. doi:10.1029/2011gb004114

Griffin, B. A., and J. J. Jurinak. 1973. Estimation of activity coefficients from the electrical conductivity of natural aquatic systems and soil extracts. Soil Sci. **116**: 26–30. doi:10.1097/00010694-197307000-00005

Herczeg, A. L., and R. H. Hesslein. 1984. Determination of hydrogen ion concentration in softwater lakes using carbon dioxide equilibria. Geochim. Cosmochim. Acta **48**: 837–845. doi:10.1016/0016-7037(84)90105-4

Hotchkiss, E. R., R. O. Hall Jr., R. A. Sponseller, D. Butman, J. Klaminder, H. Laudon, M. Rosvall, and J. Karlsson. 2015. Sources of and processes controlling CO_2 emissions change with the size of streams and rivers. Nat. Geosci. **8**: 696–699. doi:10.1038/ngeo2507

Huang, J., F. Yuan, G. Zeng, X. Li, Y. Gu, L. Shi, W. Liu, and Y. Shi. 2017. Influence of pH on heavy metal speciation and removal from wastewater using micellar-enhanced ultrafiltration. Chemosphere **173**: 199–206. doi:10.1016/j.chemosphere.2016.12.137

Hunt, C. W., J. E. Salisbury, and D. Vandemark. 2011. Contribution of non-carbonate anions to total alkalinity and overestimation of pCO_2 in New England and New Brunswick rivers. Biogeosciences **8**: 3069–3076. doi:10.5194/bg-8-3069-2011

Illingworth, J. A. 1981. A common source of error in pH measurements. Biochem. J. **195**: 259–262. doi:10.1042/bj1950259

Johnson, M. S., M. F. Billett, K. J. Dinsmore, M. Wallin, K. E. Dyson, and R. S. Jassal. 2009. Direct and continuous measurement of dissolved carbon dioxide in freshwater aquatic systems-method and applications. Ecohydrology **3**: 68–78. doi:10.1002/eco.95

Kanuri, V. V., D. R. Gijjapu, K. Munnooru, A. Sura, S. Patra, R. R. Vinjamuri, and R. Karri. 2017. Scales and drivers of seasonal pCO_2 dynamics and net ecosystem exchange along the coastal waters of southeastern Arabian Sea. Mar. Pollut. Bull. **121**: 372–380. doi:10.1016/j.marpolbul.2017.06.016

Khan, H., A. Laas, R. Marcé, M. Sepp, and B. Obrador. 2021. Eutrophication and geochemistry drive pelagic calcite precipitation in lakes. Water **13**: 597. doi:10.3390/w13050597

Lai, C.-Z., and others. 2016. Spectrophotometric measurement of freshwater pH with purified meta-cresol purple and phenol red. Limnol. Oceanogr. Methods **15**: 903. doi:10.1002/lom3.10210

Lewis, E., and D. W. R. Wallace. 1998. Program developed for CO_2 system calculations. ORNL/CDIAC-105. Carbon Dioxide Information Analysis Center, Oak Ridge National Laboratory, U.S. Department of Energy. doi:10.3334/CDIAC/otg.CO2SYS_DOS_CDIAC105

Li, X., M. I. García-Ibáñez, B. R. Carter, B. Chen, Q. Li, R. A. Easley, and W.-J. Cai. 2020. Purified meta-cresol purple dye perturbation: How it influences spectrophotometric pH measurements. Mar. Chem. **225**: 103849. doi:10.1016/j.marchem.2020.103849

Liu, S., D. E. Butman, and P. A. Raymond. 2020. Evaluating CO_2 calculation error from organic alkalinity and pH measurement error in low ionic strength freshwaters. Limnol. Oceanogr. Methods **18**: 606–622. doi:10.1002/lom3.10388

Liu, X., M. C. Patsavas, and R. H. Byrne. 2011. Purification and characterization of meta-cresol purple for spectrophotometric seawater pH measurements. Environ. Sci. Technol. **45**: 4862–4868. doi:10.1021/es200665d

Lueker, T. J., A. G. Dickson, and C. D. Keeling. 2000. Ocean pCO_2 calculated from dissolved inorganic carbon, alkalinity, and equations for K_1 and K_2: Validation based on laboratory measurements of CO_2 in gas and seawater at equilibrium. Mar. Chem. **70**: 105–119. doi:10.1016/s0304-4203(00)00022-0

Lynch, J. K., C. M. Beatty, M. P. Seidel, L. J. Jungst, and M. D. DeGrandpre. 2010. Controls of riverine CO_2 over an annual cycle determined using direct, high temporal resolution pCO_2 measurements. J. Geophys. Res. **115**: 1–10. doi:10.1029/2009jg001132

Martz, T. R., J. J. Carr, C. R. French, and M. D. DeGrandpre. 2003. A submersible autonomous sensor for spectrophotometric pH measurements of natural waters. Anal. Chem. **75**: 1844–1850. doi:10.1021/ac020568l

Millero, F. J. 1979. The thermodynamics of the carbonate system in seawater. Geochim. Cosmochim. Acta **43**: 1651–1661. doi:10.1016/0016-7037(79)90184-4

Minor, E. C., C. J. Tennant, and E. T. Brown. 2019. A seasonal to interannual view of inorganic and organic carbon and pH in western Lake Superior. J. Geophys. Res. Biogeo. **124**: 405–419. doi:10.1029/2018jg004664

Müller, B., J. S. Meyer, and R. Gächter. 2015. Alkalinity regulation in calcium carbonate-buffered lakes. Limnol. Oceanogr. **61**: 341–352. doi:10.1002/lno.10213

Müller, J. D., B. Schneider, S. Aßmann, and G. Rehder. 2017. Spectrophotometric pH measurements in the presence of dissolved organic matter and hydrogen sulfide. Limnol. Oceanogr. Methods **16**: 68–82. doi:10.1002/lom3.10227

Nagorski, S. A. 2001. Spatial and temporal variations in the geochemistry of several western Montana streams and rivers. Graduate Student Theses, Dissertations, & Professional Papers: 9408. Available from: https://scholarworks.umt.edu/etd/9408

Oren, R. A. M., C. -I. Hsieh, P. Stoy, J. Albertson, H. R. McCarthy, P. Harrell, and G. G. Katul. 2006. Estimating the uncertainty in annual net ecosystem carbon exchange: Spatial variation in turbulent fluxes and sampling errors in eddy-covariance measurements. Glob. Chang. Biol. **12**: 883–896. doi:10.1111/j.1365-2486.2006.01131.x

Parker, S. R., C. H. Gammons, S. R. Poulson, and M. D. DeGrandpre. 2007. Diel variations in stream chemistry and isotopic composition of dissolved inorganic carbon, upper Clark Fork River, Montana, USA. Appl. Geochem. **22**: 1329–1343. doi:10.1016/j.apgeochem.2007.02.007

Parkhurst, D. L., and C. A. J. Appelo. 2013. Description of input and examples for PHREEQC version 3: A computer program for speciation, batch-reaction, one-dimensional transport, and inverse geochemical calculations. Techniques and methods. U.S. Geological Survey. doi:10.3133/tm6a43

Peter, H., G. A. Singer, C. Preiler, P. Chifflard, G. Steniczka, and T. J. Battin. 2014. Scales and drivers of temporal pCO_2 dynamics in an Alpine stream. J. Geophys. Res. Biogeosci. **119**: 1078–1091. doi:10.1002/2013jg002552

Phillips, J., G. McKinley, V. Bennington, H. Bootsma, D. Pilcher, R. Sterner, and N. Urban. 2015. The potential for CO_2-induced acidification in freshwater: A Great Lakes case study. Oceanography **25**: 136–145. doi:10.5670/oceanog.2015.37

Plummer, L. N., and E. Busenberg. 1982. The solubilities of calcite, aragonite and vaterite in CO_2-H_2O solutions between 0 and 90°C, and an evaluation of the aqueous model for the system $CaCO_3$-CO_2-H_2O. Geochim. Cosmochim. Acta **46**: 1011–1040. doi:10.1016/0016-7037(82)90056-4

Raymond, P. A., N. F. Caraco, and J. J. Cole. 1997. Carbon dioxide concentration and atmospheric flux in the Hudson River. Estuaries **20**: 381. doi:10.2307/1352351

Raymond, P. A., J. E. Bauer, and J. J. Cole. 2000. Atmospheric CO_2 evasion, dissolved inorganic carbon production, and net heterotrophy in the York River estuary. Limnol. Oceanogr. **45**: 1707–1717. doi:10.4319/lo.2000.45.8.1707

Raymond, P. A., and others. 2012. Scaling the gas transfer velocity and hydraulic geometry in streams and small rivers. Limnol. Oceanogr. Fluids Environ. **2**: 41–53. doi:10.1215/21573689-1597669

Raymond, P. A., and others. 2013. Global carbon dioxide emissions from inland waters. Nature **503**: 355–359. doi:10.1038/nature12760

Rocher-Ros, G., R. A. Sponseller, W. Lidberg, C. M. Mörth, and R. Giesler. 2019. Landscape process domains drive patterns of CO_2 evasion from river networks. Limnol. Oceanogr. Lett. **4**: 87–95. doi:10.1002/lol2.10108

Rocher-Ros, G., R. A. Sponseller, A. K. Bergström, M. Myrstener, and R. Giesler. 2020. Stream metabolism controls diel patterns and evasion of CO_2 in Arctic streams. Glob. Chang. Biol. **26**: 1400–1413. doi:10.1111/gcb.14895

Rocher-Ros, G., T. K. Harms, R. A. Sponseller, M. Väisänen, C. M. Mörth, and R. Giesler. 2021. Metabolism overrides photo-oxidation in CO_2 dynamics of Arctic permafrost streams. Limnol. Oceanogr. **66**: 169–181. doi:10.1002/lno.11564

Seidel, M. P., M. D. DeGrandpre, and A. G. Dickson. 2008. A sensor for in situ indicator-based measurements of seawater pH. Mar. Chem. **109**: 18–28. doi:10.1016/j.marchem.2007.11.013

Shangguan, Q., C. Z. Lai, C. M. Beatty, F. L. Young, R. S. Spaulding, and M. D. DeGrandpre. 2021. Autonomous in situ measurements of freshwater alkalinity. Limnol.Oceanogr. Methods **19**: 51–66. doi:10.1002/lom3.10404

Stauffer, R. E. 1990. Electrode pH error, seasonal epilimnetic pCO_2, and the recent acidification of the Maine lakes. Water Air Soil Pollut. **50**: 123–148. doi:10.1007/bf00284788

Stets, E. G., D. Butman, C. P. McDonald, S. M. Stackpoole, M. D. DeGrandpre, and R. G. Striegl. 2017. Carbonate buffering and metabolic controls on carbon dioxide in rivers. Global Biogeochem. Cycles **31**: 663–677. doi:10.1002/2016gb005578

Stumm, W., and J. J. Morgan. 2008. Aquatic chemistry. Wiley.

Takeshita, Y., K. S. Johnson, L. J. Coletti, H. W. Jannasch, P. M. Walz, and J. K. Warren. 2020. Assessment of pH dependent errors in spectrophotometric pH measurements of seawater. Mar. Chem. **223**: 103801. doi:10.1016/j.marchem.2020.103801

Ulseth, A. J., R. O. Hall, M. Boix Canadell, H. L. Madinger, A. Niayifar, and T. J. Battin. 2019. Distinct air–water gas exchange regimes in low- and high-energy streams. Nat. Geosci. **12**: 259–263. doi:10.1038/s41561-019-0324-8

U.S. EPA. 2005. Method 415.3: Measurement of total organic carbon, dissolved organic carbon, and specific UV absorbance at 254 nm in source water and drinking water. Environmental Monitoring Systems Laboratory, Office of Research and Development.

Wang, Z., J. P. Meador, and K. M. Y. Leung. 2016. Metal toxicity to freshwater organisms as a function of pH: A meta-analysis. Chemosphere **144**: 1544–1552. doi:10.1016/j.chemosphere.2015.10.032

Wang, Z. A., and W.-J. Cai. 2004. Carbon dioxide degassing and inorganic carbon export from a marsh-dominated estuary (the Duplin River): A marsh CO_2 pump. Limnol. Oceanogr. **49**: 341–354. doi:10.4319/lo.2004.49.2.0341

Wang, Z. A., and others. 2019. Advancing observation of ocean biogeochemistry, biology, and ecosystems with cost-effective in situ sensing technologies. Front. Mar. Sci. **6**: 1–22. doi:10.3389/fmars.2019.00519

Weiss, R. F. 1974. Carbon dioxide in water and seawater: The solubility of a non-ideal gas. Mar. Chem. **2**: 203–215. doi:10.1016/0304-4203(74)90015-2

Wen, Z., K. Song, Y. Shang, C. Fang, L. Li, L. Lv, X. Lv, and L. Chen. 2017. Carbon dioxide emissions from lakes and reservoirs of China: A regional estimate based on the calculated pCO_2. Atmos. Environ. **170**: 71–81. doi:10.1016/j.atmosenv.2017.09.032

Wilcock, R. J., and S. C. Chapra. 2005. Diel changes of inorganic chemistry in a macrophyte-dominated, softwater stream. Mar. Freshw. Res. **56**: 1165. doi:10.1071/mf05049

Yang, B., M. C. Patsavas, R. H. Byrne, and J. Ma. 2014. Seawater pH measurements in the field: A DIY photometer with 0.01 unit pH accuracy. Mar. Chem. **160**: 75–81. doi:10.1016/j.marchem.2014.01.005

Yao, W., and R. H. Byrne. 2001. Spectrophotometric determination of freshwater pH using bromocresol purple and phenol red. Environ. Sci. Technol. **35**: 1197–1201. doi:10.1021/es001573e

Yao, W., X. Liu, and R. H. Byrne. 2007. Impurities in indicators used for spectrophotometric seawater pH measurements: Assessment and remedies. Mar. Chem. **107**: 167–172. doi:10.1016/j.marchem.2007.06.012

Young, F.L., Shangguan, Q., Beatty, C.M., Gilsdorf, M.D., and DeGrandpre, M.D. (2022). 2018–2020 Laboratory measurements of inorganic carbon accompanied by sensor data measurements of in situ inorganic carbon from the Upper Clark Fork River (Montana, USA) version 1. Environmental Data Initiative. doi:10.6073/pasta/c3bd7a65cfafa464b89857c5e375d20d.

Yuan, S., and M. D. DeGrandpre. 2008. Evaluation of indicator-based pH measurements for freshwater over a wide range of buffer intensities. Environ. Sci. Technol. **42**: 6092–6099. doi:10.1021/es800829x

Zhang, H., and R. H. Byrne. 1996. Spectrophotometric pH measurements of surface seawater at in-situ conditions: Absorbance and protonation behavior of thymol blue. Mar. Chem. **52**: 17–25. doi:10.1016/0304-4203(95)00076-3

Acknowledgments

The authors thank the H. M. Valett research group at the University of Montana for help with sample collection. The authors thank Venice Bayrd and Robert Payn for their help with data curation and to the anonymous reviewers for their constructive and valued feedback. This research was supported in part by the U.S. National Science Foundation Long Term Research in Environmental Biology program (DEB-1655197), Montana NSF EPSCoR program (OIA-1757351), and the University of Montana through a teaching assistantship to Fischer L. Young. The data and processing code underlying this manuscript provide laboratory and in situ sensor measurements of inorganic carbon parameters for the purpose of calculating freshwater pCO_2. The data and code can be found on the Environmental Data Initiative (EDI) repository using the following DOI: 10.6073/pasta/c3bd7a65cfafa464b89857c5e375d20d. Registration with EDI is not required to access these data. All data and code are released with a public domain waiver, CC0 1.0 Universal (CC0 1.0), though attribution via citation is expected if the data or code are reused, as per scholarly convention. Preferred citation information can be found in the "References" section (Young et al. 2022).

Conflict of Interest

Michael D. DeGrandpre is a co-owner of Sunburst Sensors, LLC, the company that manufactures the SAMI sensor technologies.

Submitted 18 January 2022
Revised 16 June 2022
Accepted 17 June 2022

Associate editor: Isaac Santos

Supporting Information for

Title:

Comparison of spectrophotometric and electrochemical pH measurements for calculating freshwater pCO_2

Authors:

Fischer L. Young[1], Qipei Shangguan[1], Cory M. Beatty[1], Makenzy D. Gilsdorf[1], and Michael D. DeGrandpre[1*]

[1]Department of Chemistry and Biochemistry, University of Montana, Missoula, Montana, USA

*Corresponding author

Email: michael.degrandpre@umontana.edu; telephone: (406) 243-4118

Running head:

Comparing pH for calculating pCO_2

Keywords:

freshwater, spectrophotometric pH, electrochemical pH, partial pressure of carbon dioxide, inorganic carbon, ionic strength

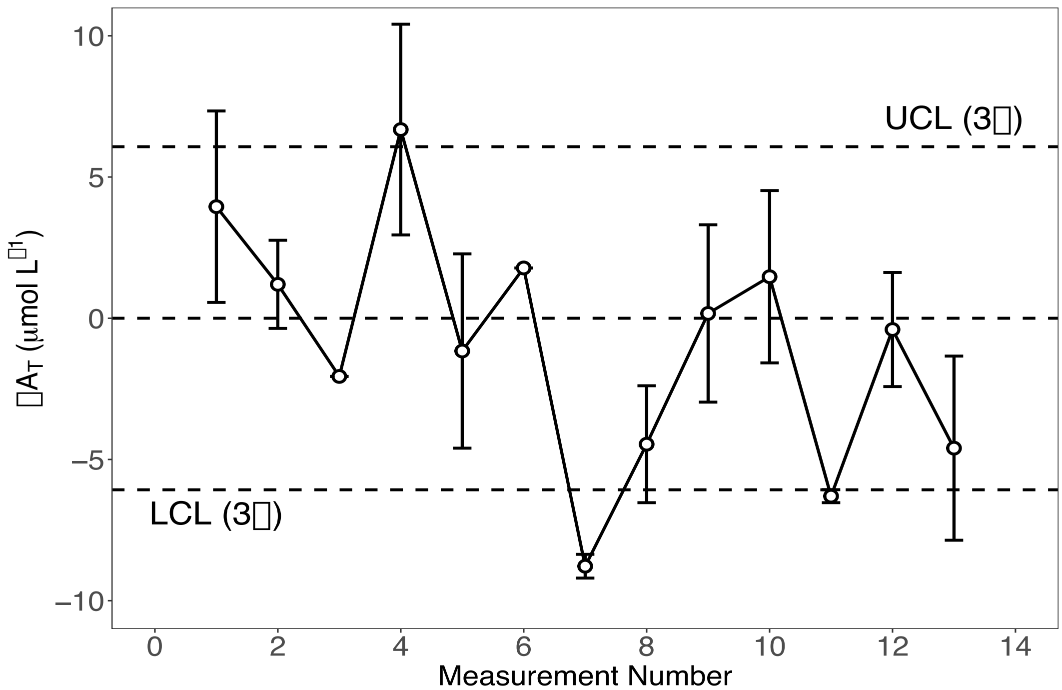

Fig. S1. The A_T quality control chart representing the differences between known A_T standard values and measured A_T values. ΔA_T represents the average error between the known and measured A_T values (measured – known). The average ΔA_T is -1.0 ± 4.3 µmol L^{-1} (n = 13). The UCL and LCL represent the upper and lower 99% control limits, respectively, calculated from three times the average measurement standard deviation. Error bars represent the standard deviation of replicates. A total of 13 measurements were made covering the duration of the tank study experiment as outlined in the main text.

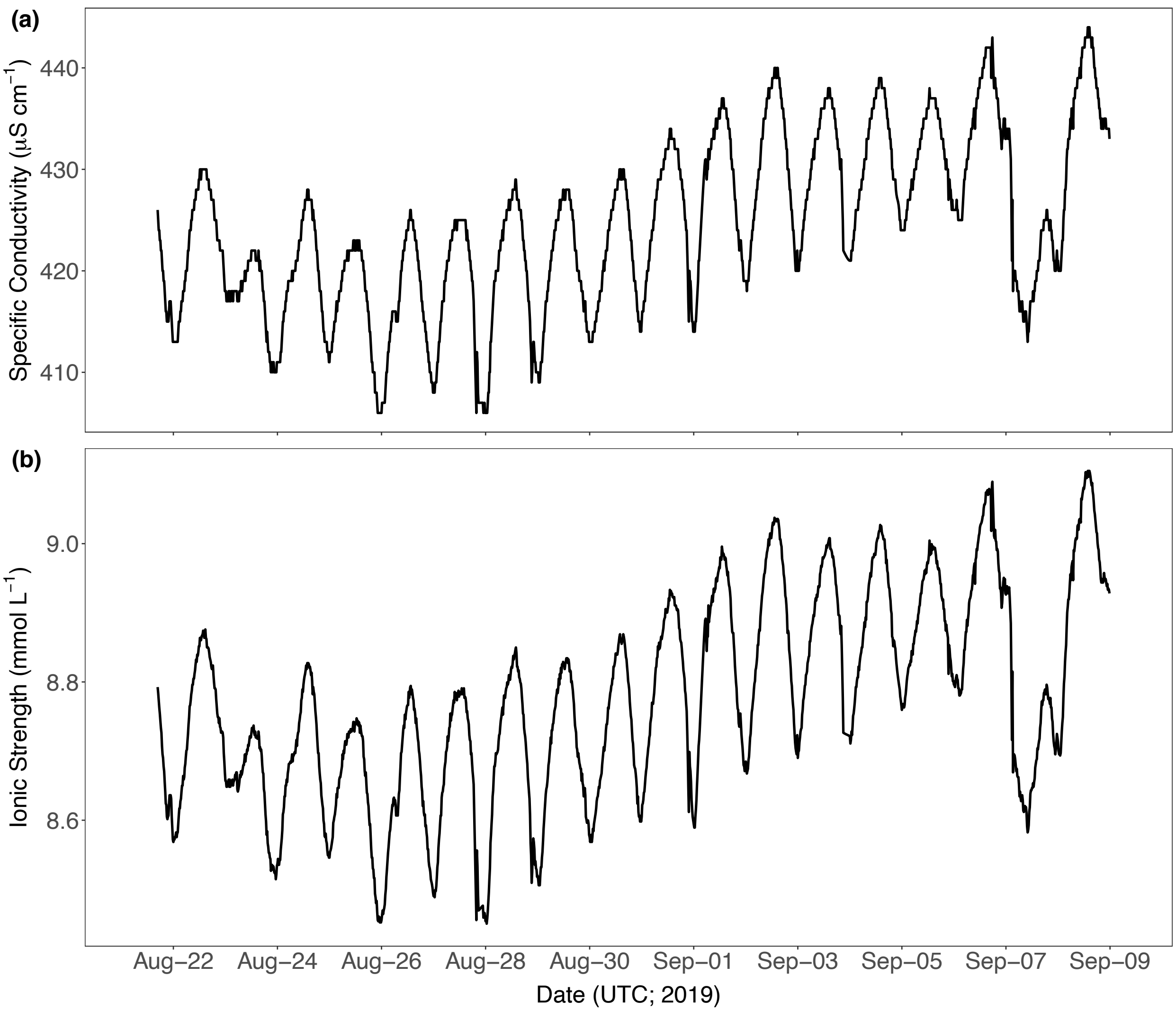

Fig. S2. A 19-day time series from the CFR of **(a)** measured specific conductivity and **(b)** calculated ionic strength. Ionic strength was calculated using the conductivity-derived A_T obtained from Figure 1 in the main text along with eq. 5 (Nagorski 2020). The date and time are UTC during the year 2019.

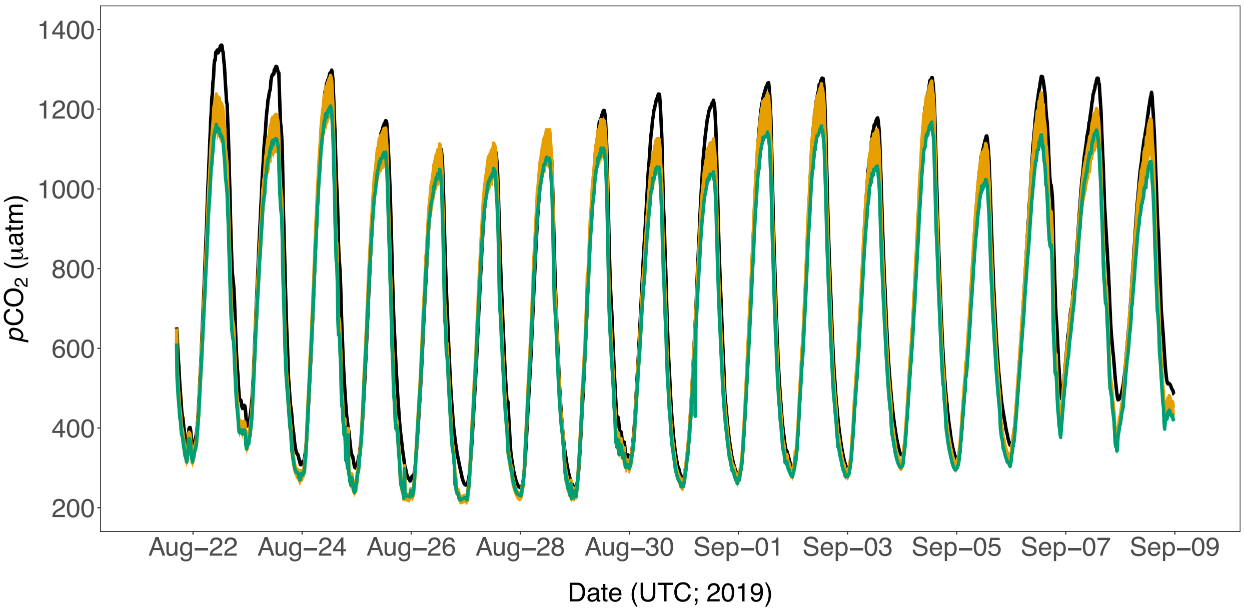

Fig. S3. Measured (solid black line) pCO_2 time series compared to calculated pCO_2 using conductivity-derived A_T with ±130 µmol L^{-1} uncertainty limits (orange ribbon) and calculated pCO_2 using a constant A_T (3050 µmol L^{-1}) (green line). This plot examines the uncertainty in the conductivity derived A_T relationship and how it can help explain the observed difference between measured and calculated pCO_2 in Figure 6d of the main text.

Table S1. Example spectrophotometric pH_{free} measurements with molar absorptivity (ε), absorbances (A), and indicator concentrations used in the pH_{free} calculation (Eq. 1 of the main text). Samples 1 and 2 were measured at similar temperatures but different pCO_2 levels (~100 and ~1600 µatm, respectively). Each molar absorptivity is distinguished by wavelength (434 or 578) and form of the indicator species (i.e., a = acidic form (HI^-) and b = basic form (I^{2-})). The perturbation free pH was determined by the y-intercept of the regression between total indicator concentration and pH, as outlined in the main text.

Sample	Temp (°C)	εa434 (L mol^{-1} cm^{-1})	εa578 (L mol^{-1} cm^{-1})	εb434 (L mol^{-1} cm^{-1})	εb578 (L mol^{-1} cm^{-1})	A434	A578	HI^- (M)	I^{2-} (M)	Total Indicator Concentration (M)	pK_a	pH	Perturbation Free pH
1A	14.88	18000	103	2078	41845	0.0981	0.4917	4.06E-06	1.17E-05	1.58E-05	8.7612	9.0621	9.0641
1B	14.87	18000	103	2078	41846	0.1962	0.9857	8.19E-06	2.35E-05	3.17E-05	8.7613	9.0600	
1C	14.86	18001	103	2078	41847	0.2951	1.4740	1.23E-05	3.52E-05	4.75E-05	8.7614	9.0580	
2A	15.37	17984	103	2081	41790	0.2243	0.1417	1.21E-05	3.35E-06	1.54E-05	8.7561	8.0397	8.0413
2B	15.35	17984	103	2081	41792	0.4530	0.2847	2.44E-05	6.74E-06	3.11E-05	8.7563	8.0378	
2C	15.32	17985	103	2081	41796	0.6855	0.4293	3.69E-05	1.01E-05	4.70E-05	8.7566	8.0363	

Table S2. The average, standard deviation, and sample sizes for specific conductivity, total alkalinity (A_T), several ions used to calculate ionic strength (i.e., calcium, magnesium, chloride, and sulfate) (Eq. 4 of the main text), and the resulting estimated ionic strength during the duration of the tank study. Averages and standard deviations represent all treatments for the duration of the tank study experiment, as outlined in the main text. A counterion (Na^+) at a concentration of 0.07 mmol L^{-1} was used to achieve charge balance.

	Specific Conductivity (µS cm^{-1})	A_T (µmol L^{-1})	Calcium (mg L^{-1})	Magnesium (mg L^{-1})	Chloride (mg L^{-1})	Sulfate (mg L^{-1})	Ionic Strength (mmol L^{-1})
Average	334	2806	57	19	28	21	7.5
SD	54	395	8	3	4	3	1.1
n	35	34	35	35	35	35	35

Appendix A

Below is the code used in the main text for calculating freshwater pCO$_2$ from pH$_{free}$, A$_T$, temperature, and ionic strength. In the main text this program is referred to as “CalcCO2_frompH”. Commented throughout the code are references and descriptions for how to use the code.

```
% ****************pCO2_Equilibrium_Model_TA_pH_freshwater.M******************
% **********ORIGINALLY WRITTEN BY T.MARTZ FOR SEAWATER***************
% *******************MODIFIED FOR FRESHWATER BY C.LAI******************
% ****************MODIFIED FOR READING DATASETS BY F. YOUNG************
% *******PROGRAM FOR CALCULATING pCO2 from pH and TA for freshwater********
% ******** Copyright 2022 - Martz, Lai, Young, and DeGrandpre.  MIT License ***********

%~~~~~~~~~~~~~~~~~~~~~~~~~~~~~~~~~~~~~~~~~~~~~~~~~~~~~~~~~~~~~~~~~~
%Brief Description of Program
%~~~~~~~~~~~~~~~~~~~~~~~~~~~~~~~~~~~~~~~~~~~~~~~~~~~~~~~~~~~~~~~~~~
% This program is used to calculate the partial pressure of carbon dioxide
% (pCO2) from pH and total alkalinity (TA). Ionic strength (I) is used for
% both the pH measurement and apparent equilibrium constants (K1a, K2a, KWa,
% and KHa). pH measurements are made on the Free Hydrogen Ion Scale and the
% hydrogen ion activity is determined using the Davies equation.

%~~~~~~~~~~~~~~~~~~~~~~~~~~~~~~~~~~~~~~~~~~~~~~~~~~~~~~~~~~~~~~~~~~
%Example of how to use Program
%~~~~~~~~~~~~~~~~~~~~~~~~~~~~~~~~~~~~~~~~~~~~~~~~~~~~~~~~~~~~~~~~~~
% Upload input parameters ('Temp','spCond' or 'IS, 'TA', and 'pH') as column
% vectors. Note: make sure that the units are correct as described below in
% 'INPUT VALUES'. Once input parameters are loaded and labeled properly, 'RUN'
% the script. The program will automatically generate the calculated pCO2
% under the column vector labeled 'pCO2_correction'. This will be the final
% pCO2 value. Note that this program also generates calculated values for
% dissolved inorganic carbon (DIC), bicarbonate ion (HCO3), carbonate ion (CO3),
% and dissolved CO2 (CO2).

%~~~~~~~~~~~~~~~~~~~~~~~~~~~~~~~~~~~~~~~~~~~~~~~~~~~~~~~~~~~~~~~~~~
% START SCRIPT
%~~~~~~~~~~~~~~~~~~~~~~~~~~~~~~~~~~~~~~~~~~~~~~~~~~~~~~~~~~~~~~~~~~

%~~~~~~~~~~~~~~~~~~~~~~~~~~~~~~~~~~~~~~~~~~~~~~~~~~~~~~~~~~~~~~~~~~
%Global Environment
%~~~~~~~~~~~~~~~~~~~~~~~~~~~~~~~~~~~~~~~~~~~~~~~~~~~~~~~~~~~~~~~~~~
global CT TA KWa K1a K2a KHa alpha1 alpha2

%~~~~~~~~~~~~~~~~~~~~~~~~~~~~~~~~~~~~~~~~~~~~~~~~~~~~~~~~~~~~~~~~~~
%Input Values
```

```
%~~~~~~~~~~~~~~~~~~~~~~~~~~~~~~~~~~~~~~~~~~~~~~~~~~~~~~~~~~~~~~~~~~~~~~~~~~~~~~~~~~
TC = Temp; %temperature in degrees celsius
TK = TC + 273.15; %temperature in Kelvin
EC = spCond ./ 1000; %electrical conductivity. EC must is in mS/cm so use uS/cm with the
%'./1000'
TA = TA ./ 1000000; %measured total alkalinity in mol/kg so make sure input TA is in umol/kg
pH = pH; %determined pH on the Free Hydrogen Ion Scale
I = 0.0127 .* EC; %ionic strength calculated from electrical conductivity in mol/L using Griffin
%and Jurinak 1973 relationship
%I = IS; %if ionic strength is known comment out 'EC' and 'I' calculation to use ionic strength
%estimates directly and uncomment this line.

%~~~~~~~~~~~~~~~~~~~~~~~~~~~~~~~~~~~~~~~~~~~~~~~~~~~~~~~~~~~~~~~~~~~~~~~~~~~~~~~~~~
%Calculating activity coefficients
%~~~~~~~~~~~~~~~~~~~~~~~~~~~~~~~~~~~~~~~~~~~~~~~~~~~~~~~~~~~~~~~~~~~~~~~~~~~~~~~~~~
%Calculations of concentrations for different ions are based on the equilibrium
%with the inclusion of activity coefficients and Davies equation
%~~~~~~~~~~~~~~~~~~~~~~~~~~~~~~~~~~~~~~~~~~~~~~~~~~~~~~~~~~~~~~~~~~~~~~~~~~~~~~~~~~
A = 0.5092 + (TC - 25) .* 0.00085; % temperature-related coefficient in Davies equation
gamma = -A.*(I .^ 0.5 ./ (1 + I .^ 0.5) - 0.3 .* I); % part of Davies equation
%~~~~~~~~~~~~~~~~~~~~~~~~~~~~~~~~~~~~~~~~~~~~~~~~~~~~~~~~~~~~~~~~~~~~~~~~~~~~~~~~~~
% Therefore, the activity coefficient to different ions are relevant to gamma*(charge of ion)^2
%~~~~~~~~~~~~~~~~~~~~~~~~~~~~~~~~~~~~~~~~~~~~~~~~~~~~~~~~~~~~~~~~~~~~~~~~~~~~~~~~~~
ACH = 10 .^ gamma; % activity coefficient for H+
ACOH = 10 .^ gamma; % activity coefficient for OH-
ACHCO3 = 10 .^ gamma; % activity coefficient for HCO3-
ACCO3 = 10 .^ (4 .* gamma); % activity coefficient for CO32-
%~~~~~~~~~~~~~~~~~~~~~~~~~~~~~~~~~~~~~~~~~~~~~~~~~~~~~~~~~~~~~~~~~~~~~~~~~~~~~~~~~~
%Calculating freshwater apparent equilibrium constants K1K2 (Source: Millero et al. 1979)
%~~~~~~~~~~~~~~~~~~~~~~~~~~~~~~~~~~~~~~~~~~~~~~~~~~~~~~~~~~~~~~~~~~~~~~~~~~~~~~~~~~
K1 = exp(290.9097 - 14554.21./TK - 45.0575.*log(TK));
K1a = K1 ./ (ACH .* ACHCO3); % apparent dissociation coefficient

K2 = exp(207.6548 - 11843.79./TK - 33.6485.*log(TK));
K2a = K2./(ACH .* ACCO3./ACHCO3); % apparent dissociation coefficient
%~~~~~~~~~~~~~~~~~~~~~~~~~~~~~~~~~~~~~~~~~~~~~~~~~~~~~~~~~~~~~~~~~~~~~~~~~~~~~~~~~~
%Calculating freshwater apparent equilibrium constants KW (Source: Millero 1995)
%~~~~~~~~~~~~~~~~~~~~~~~~~~~~~~~~~~~~~~~~~~~~~~~~~~~~~~~~~~~~~~~~~~~~~~~~~~~~~~~~~~
KW = exp(-13847.26 ./ TK + 148.9802 - 23.6521 .* log(TK));
KWa = KW./(ACH .* ACOH); % apparent dissociation coefficient
%~~~~~~~~~~~~~~~~~~~~~~~~~~~~~~~~~~~~~~~~~~~~~~~~~~~~~~~~~~~~~~~~~~~~~~~~~~~~~~~~~~
%Calculating freshwater apparent equilibrium constants KH (Source: Weiss 1974)
%~~~~~~~~~~~~~~~~~~~~~~~~~~~~~~~~~~~~~~~~~~~~~~~~~~~~~~~~~~~~~~~~~~~~~~~~~~~~~~~~~~
KH = exp(93.4517 .* 100 ./ TK - 60.2409 + 23.3585 .* log(TK ./ 100));

    % Convert ionic strength to salinity
```

```
                    S = 53.974*I;

KHa = KH + (0.023517 - 0.023656 * TK./100 + 0.0047036 .* TK./100 .* TK./100).*S;
%~~~~~~~~~~~~~~~~~~~~~~~~~~~~~~~~~~~~~~~~~~~~~~~~~~~~~~~~~~~~~~~~~~~~~~~~~~~~~~~
%Calculation of each ion concentration
%~~~~~~~~~~~~~~~~~~~~~~~~~~~~~~~~~~~~~~~~~~~~~~~~~~~~~~~~~~~~~~~~~~~~~~~~~~~~~~~
   H = 10.^(-pH);
   OH = KWa ./ H;
   alpha1 = (H .* K1a)./(H.^2 + K1a .* H + K1a .* K2a);
   alpha2 = (K1a .* K2a) ./ (H.^2 + K1a .* H + K1a .* K2a);
   CT  = (TA- OH + H) ./ (alpha1 + 2.*alpha2);
   CO2 = CT .* (H .^ 2) ./ (H .^ 2 + K1a .* H + K1a .* K2a);
   HCO3 = CO2 .* K1a ./ H;
   CO3 = HCO3 .* K2a ./ H;
%~~~~~~~~~~~~~~~~~~~~~~~~~~~~~~~~~~~~~~~~~~~~~~~~~~~~~~~~~~~~~~~~~~~~~~~~~~~~~~~
%DIC calculation
%~~~~~~~~~~~~~~~~~~~~~~~~~~~~~~~~~~~~~~~~~~~~~~~~~~~~~~~~~~~~~~~~~~~~~~~~~~~~~~~
DIC = CT .* 1000000;
%~~~~~~~~~~~~~~~~~~~~~~~~~~~~~~~~~~~~~~~~~~~~~~~~~~~~~~~~~~~~~~~~~~~~~~~~~~~~~~~
%pCO2 calculation
%~~~~~~~~~~~~~~~~~~~~~~~~~~~~~~~~~~~~~~~~~~~~~~~~~~~~~~~~~~~~~~~~~~~~~~~~~~~~~~~
CO2 = (CT .* (H.^2) .* 10.^ (6.*gamma)) ./ ((H.^2 .* 10.^(6.*gamma))+ (K1 .* H .*
10.^(4.*gamma))+ (K1 .* K2));

  %Uses Henry's Law constant and converts from atm to uatm (KH in fugacity (mol-atm / kg-
  %soln))
   pCO2 = (CO2 ./ KH) .* 1000000;
  %Uses the apparent Henry's Law constant and converts from atm to uatm (KHa in fugacity
  %(mol-atm / kg-soln))
   pCO2_correction = (CO2 ./ KHa) .* 1000000;

%~~~~~~~~~~~~~~~~~~~~~~~~~~~~~~~~~~~~~~~~~~~~~~~~~~~~~~~~~~~~~~~~~~~~~~~~~~~~~~~
%END SCRIPT
%~~~~~~~~~~~~~~~~~~~~~~~~~~~~~~~~~~~~~~~~~~~~~~~~~~~~~~~~~~~~~~~~~~~~~~~~~~~~~~~
```